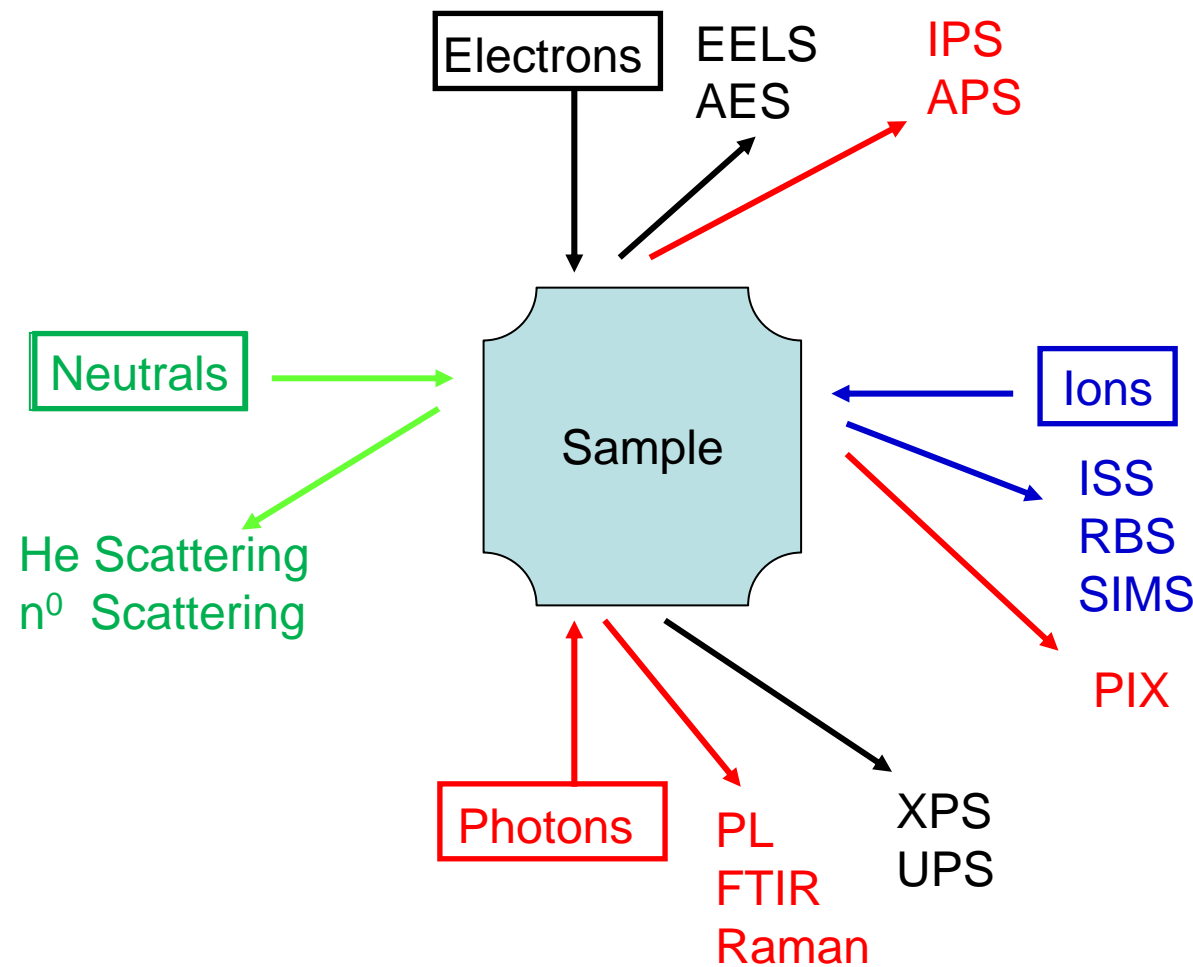


Spectroscopy at nanometer scale

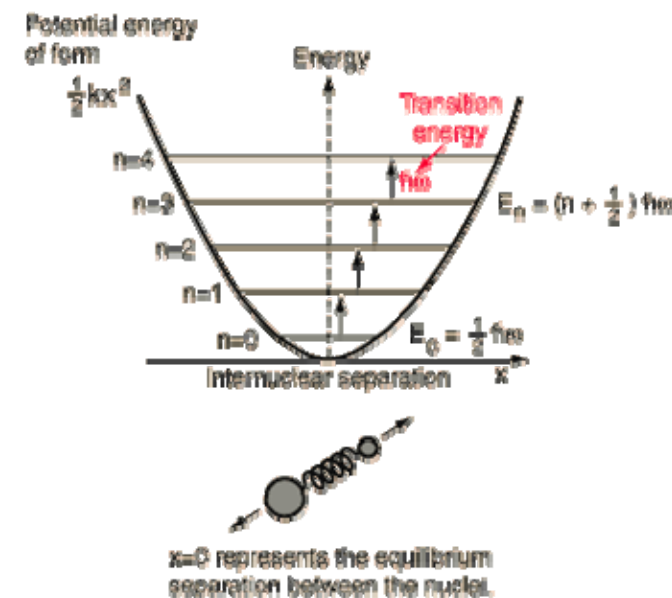
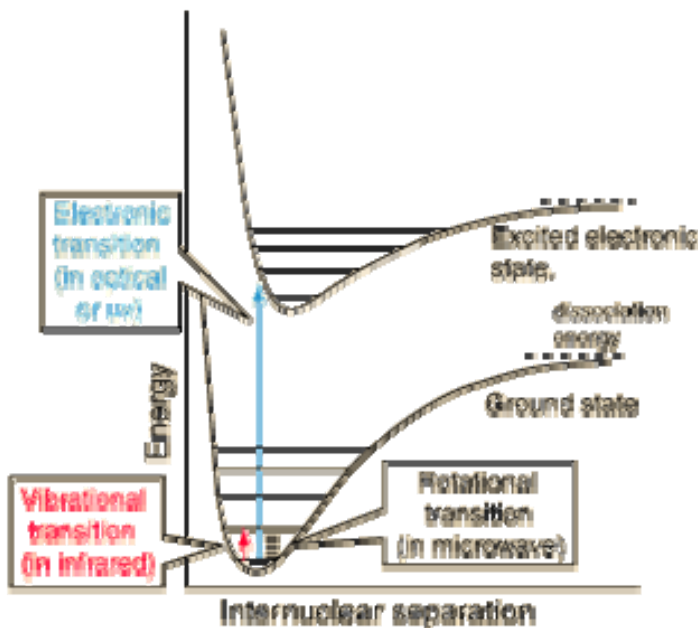
1. Physics of the spectroscopies
2. Spectroscopies for the bulk materials
3. Experimental setups for the spectroscopies
4. Physics and Chemistry of nanomaterials

Various spectroscopic methods



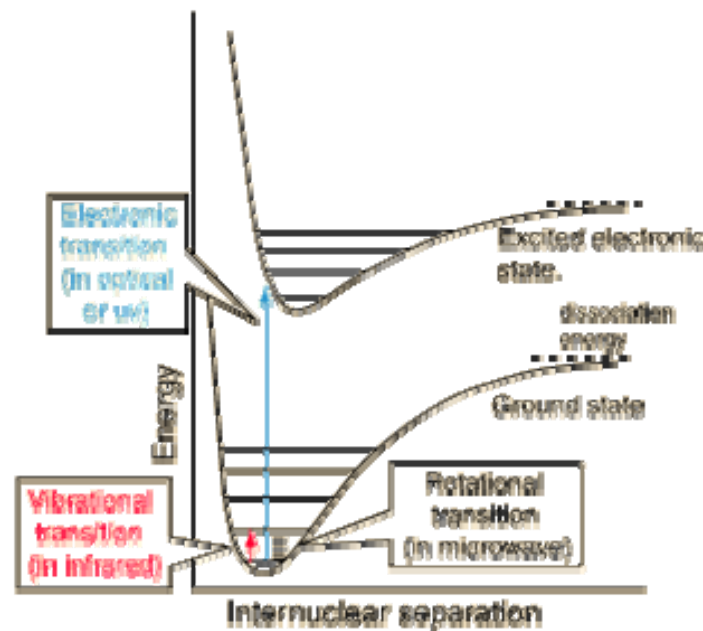
Born-Oppenheimer Approximation

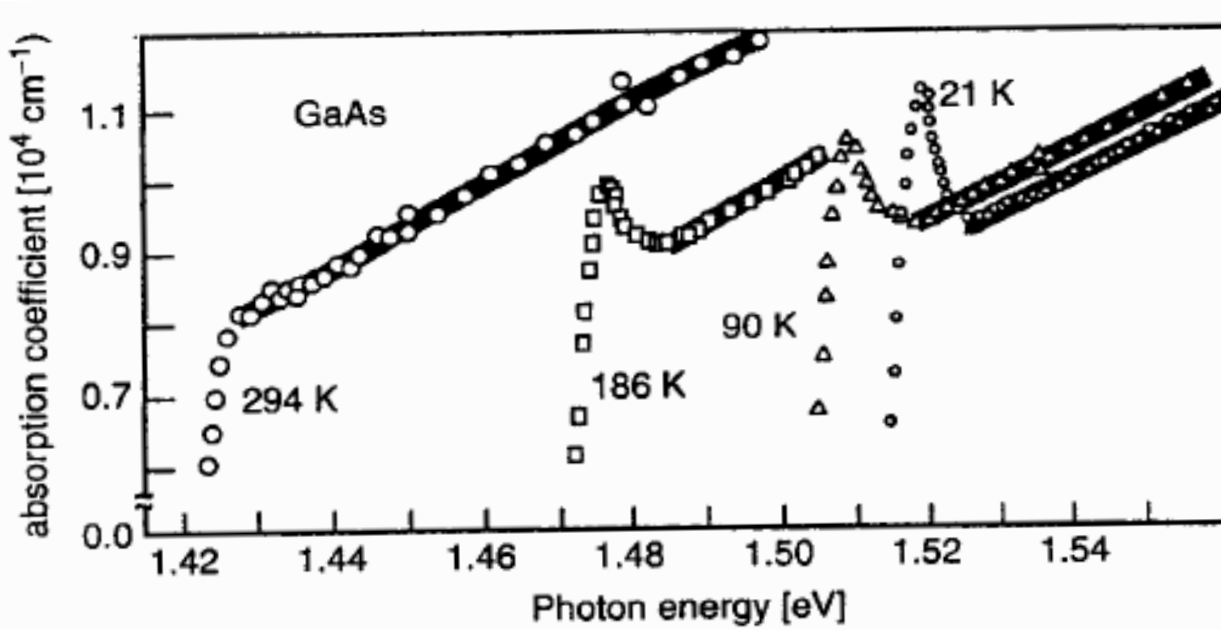
$$\Psi_{\text{molecule}}(\vec{r}_1, \vec{R}_1) = \Psi_{\text{electrons}}(\vec{r}_1, \vec{R}_1) \Psi_{\text{nuclei}}(\vec{R}_1)$$



Electronic Spectroscopy

1. Photons in, photons out – PL
2. Photons in, electrons out – UPS, XPS
3. Electrons in, electrons out – EELS





Binding energy and effective radius for the exciton

$$E_e = (m^*/m_e)(\epsilon/\epsilon_0)^{-2} \text{ (13.6 eV)}$$

$$a_{\text{eff}} = (\epsilon/\epsilon_0)(m^*/m_e)^{-1} \text{ (0.0529 nm)}$$

For GaAs, $\epsilon/\epsilon_0 \sim 13.2$ and $m^* \sim 0.067m_e$

then $E_e \sim 5 \text{ meV}$ and $a_{\text{eff}} \sim 10 \text{ nm}$

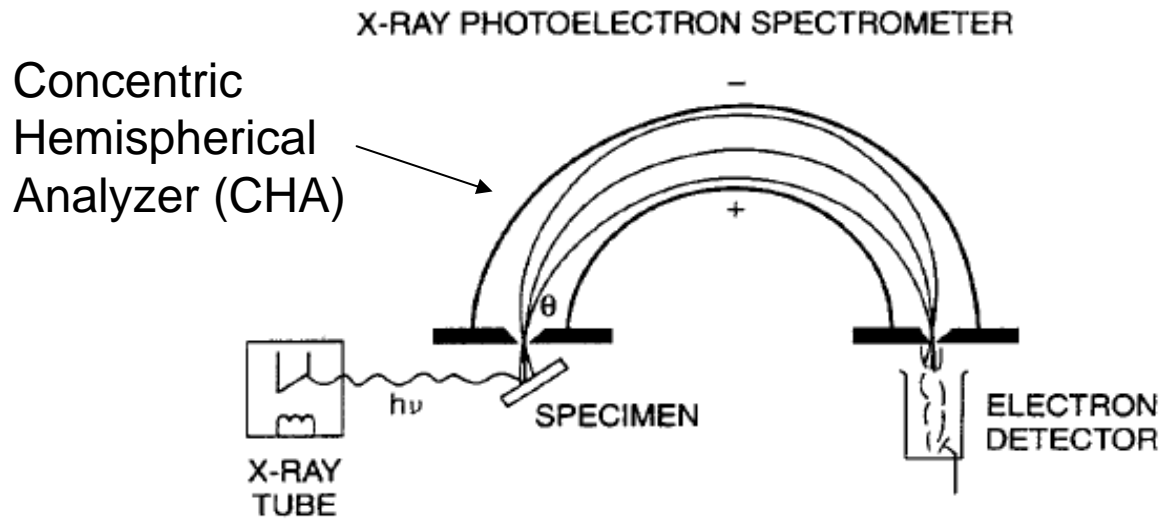
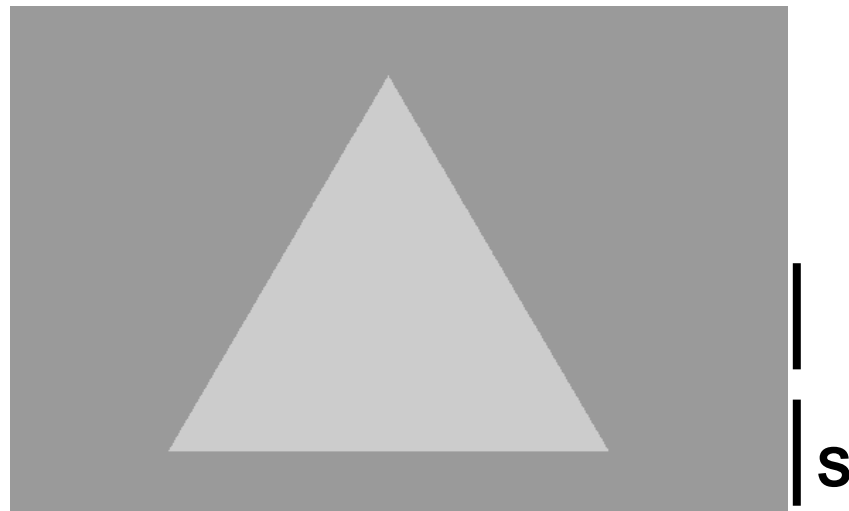
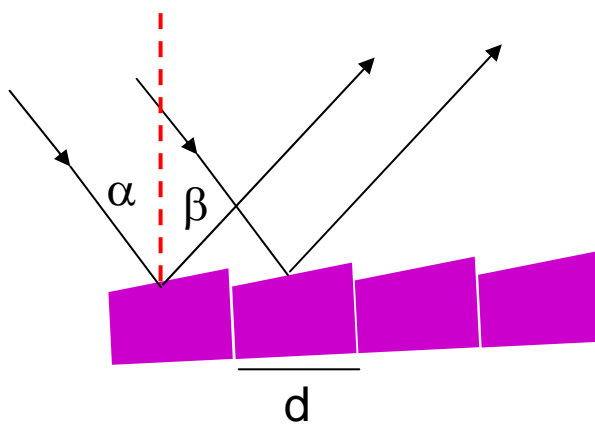


Figure 3.29. X-ray photoelectron spectrometer showing photons $h\nu$ generated by an X-ray tube incident on the specimen where they produce photoelectrons e^- characteristic of the specimen material, which then traverse a velocity analyzer, and are brought to focus at an electron detector that measures their kinetic energy.

Prism



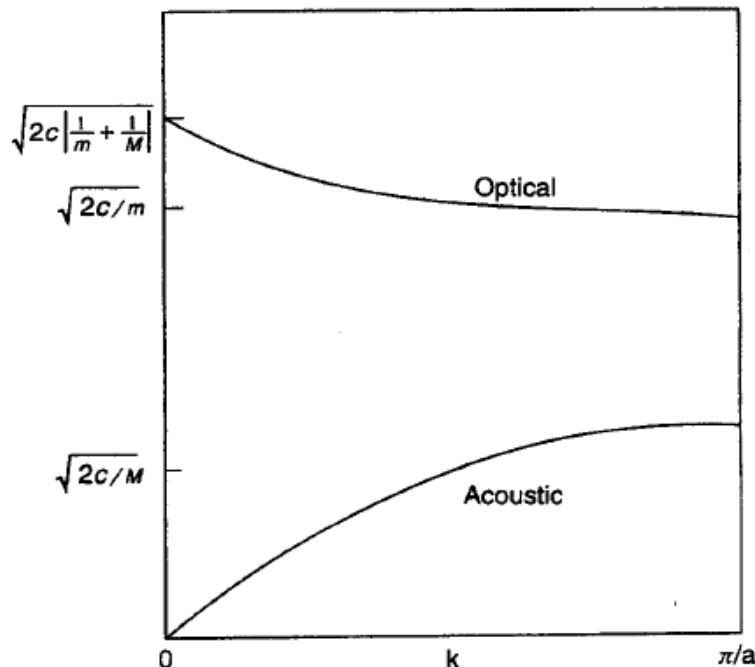
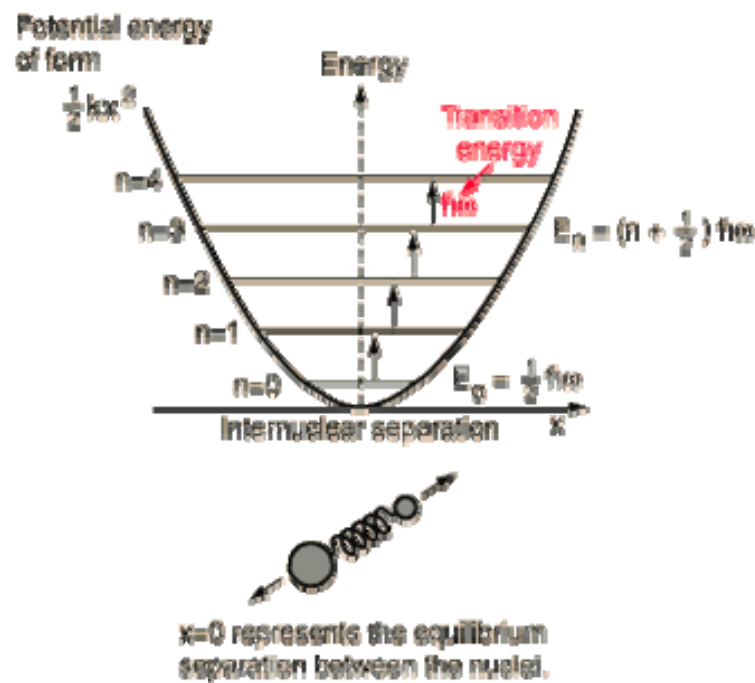
Grating



$$\Delta s = d (\sin \alpha - \sin \beta) = m\lambda$$

Vibrational Spectroscopy

1. Photons in, photons out – IR, Raman
2. Electrons in, electrons out – EELS



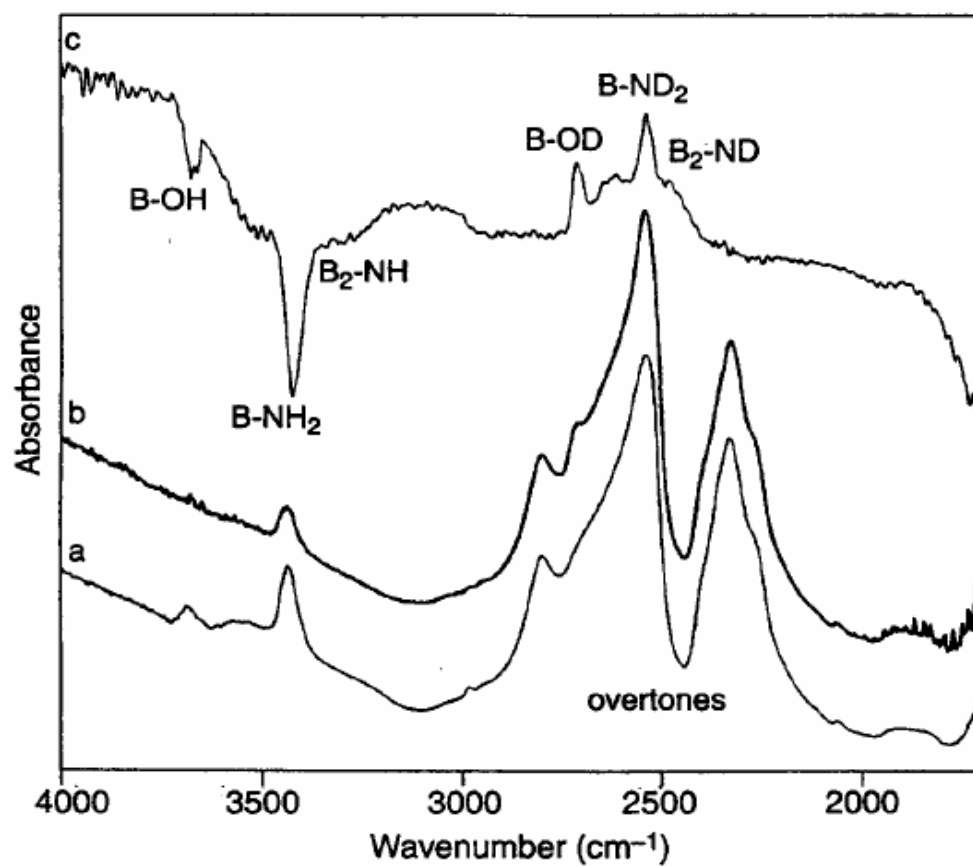
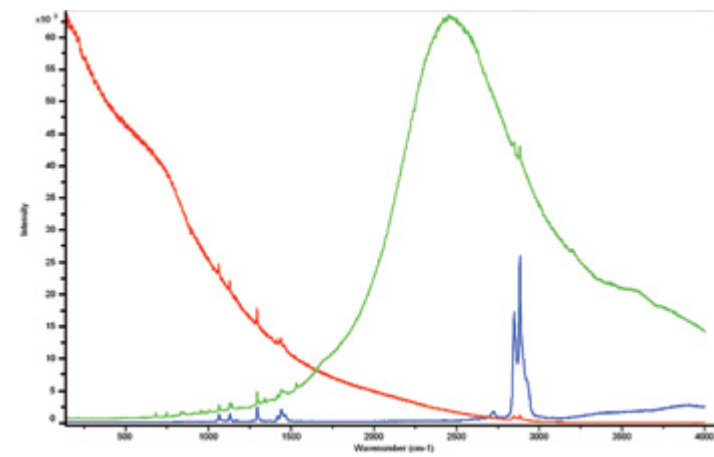
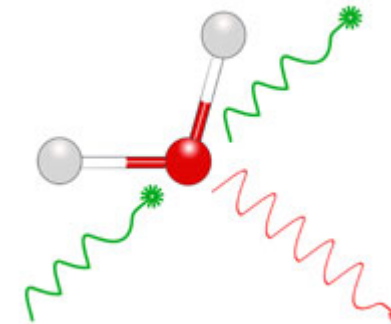
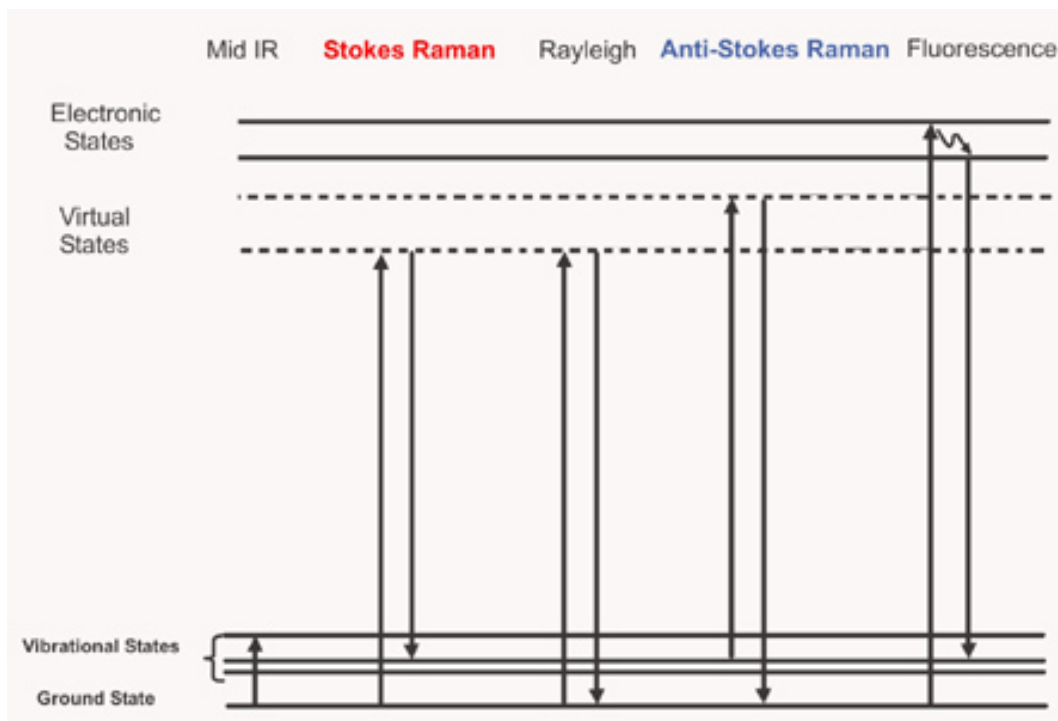


Figure 8.5. FTIR spectra of boron nitride nanopowder surfaces after activation at 875 K (tracing a), after subsequent deuteration (tracing b), and (c) difference spectrum of a subtracted from b (tracing c). [From M.-I. Baraton and L. Merhari, P. Quintard, V. Lorezenvilli, *Langmuir*, **9**, 1486 (1993).]

The Theory of Raman Spectroscopy



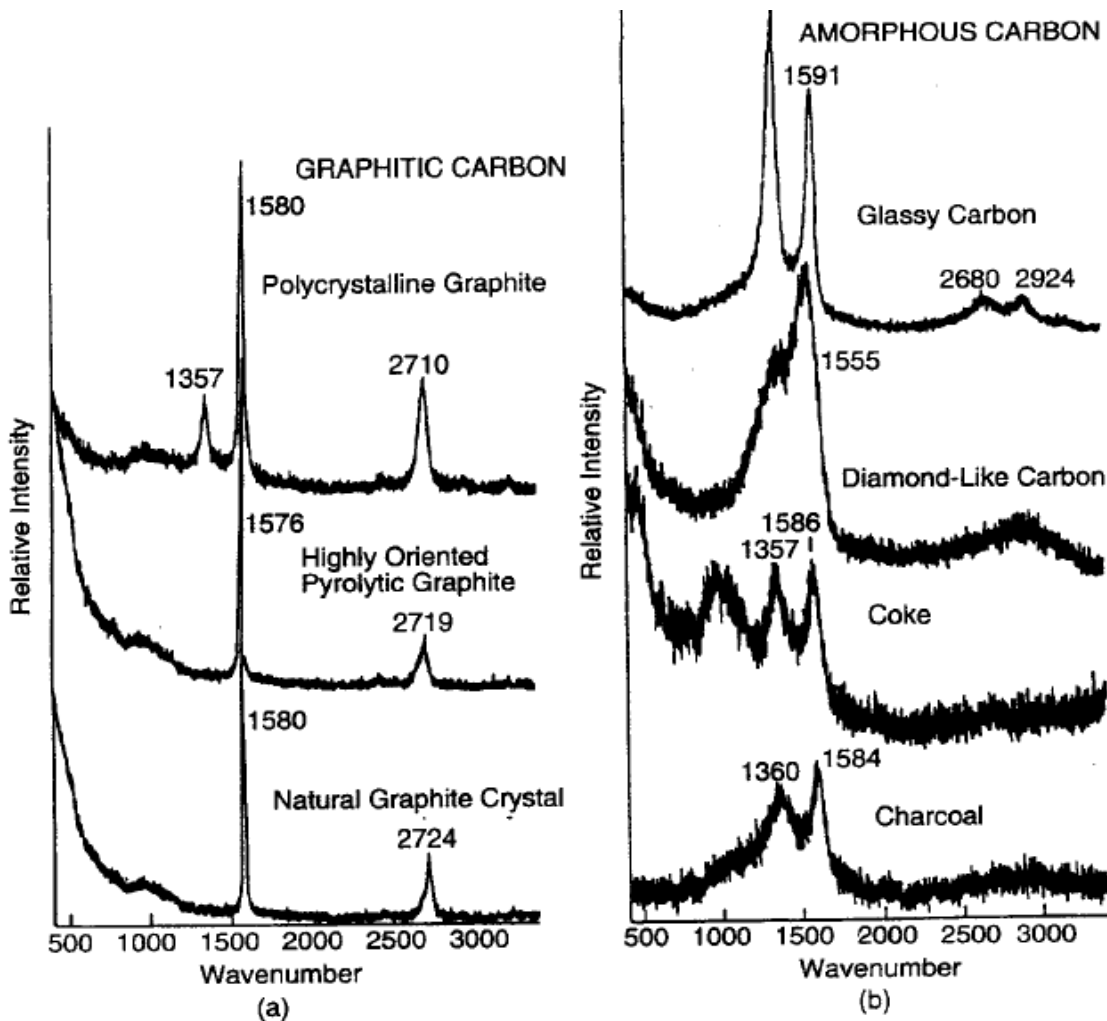
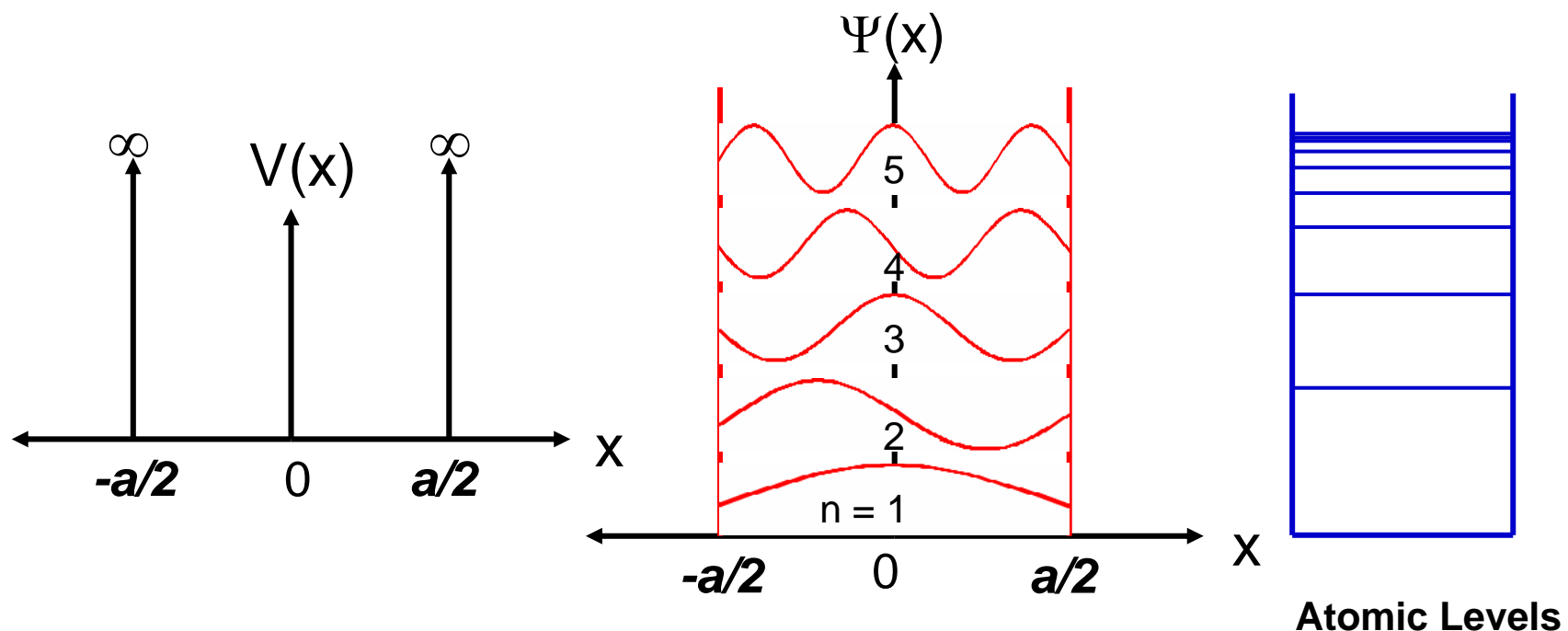


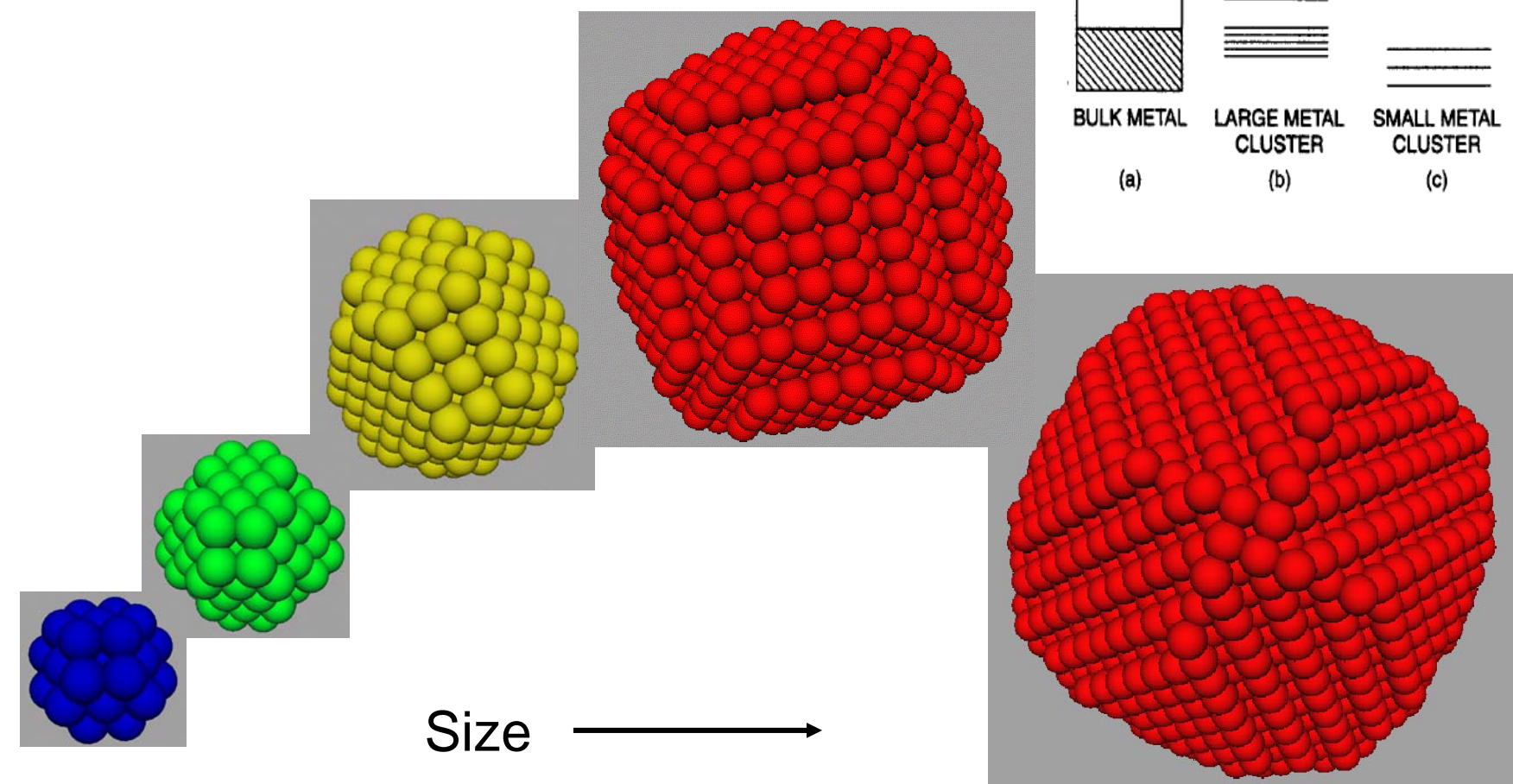
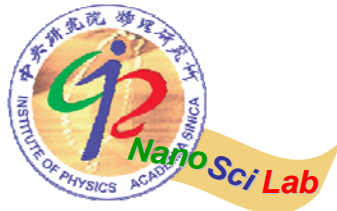
Figure 8.19. Raman spectra of (a) crystalline graphites and (b) noncrystalline, mainly graphitic, carbons. The *D* band appears near 1355cm^{-1} and the *G* band, near 1580cm^{-1} . [From D. S. Knight and W. B. White, *J. Mater. Sci.* **4**, 385 (1989).]

One dimensional size effect

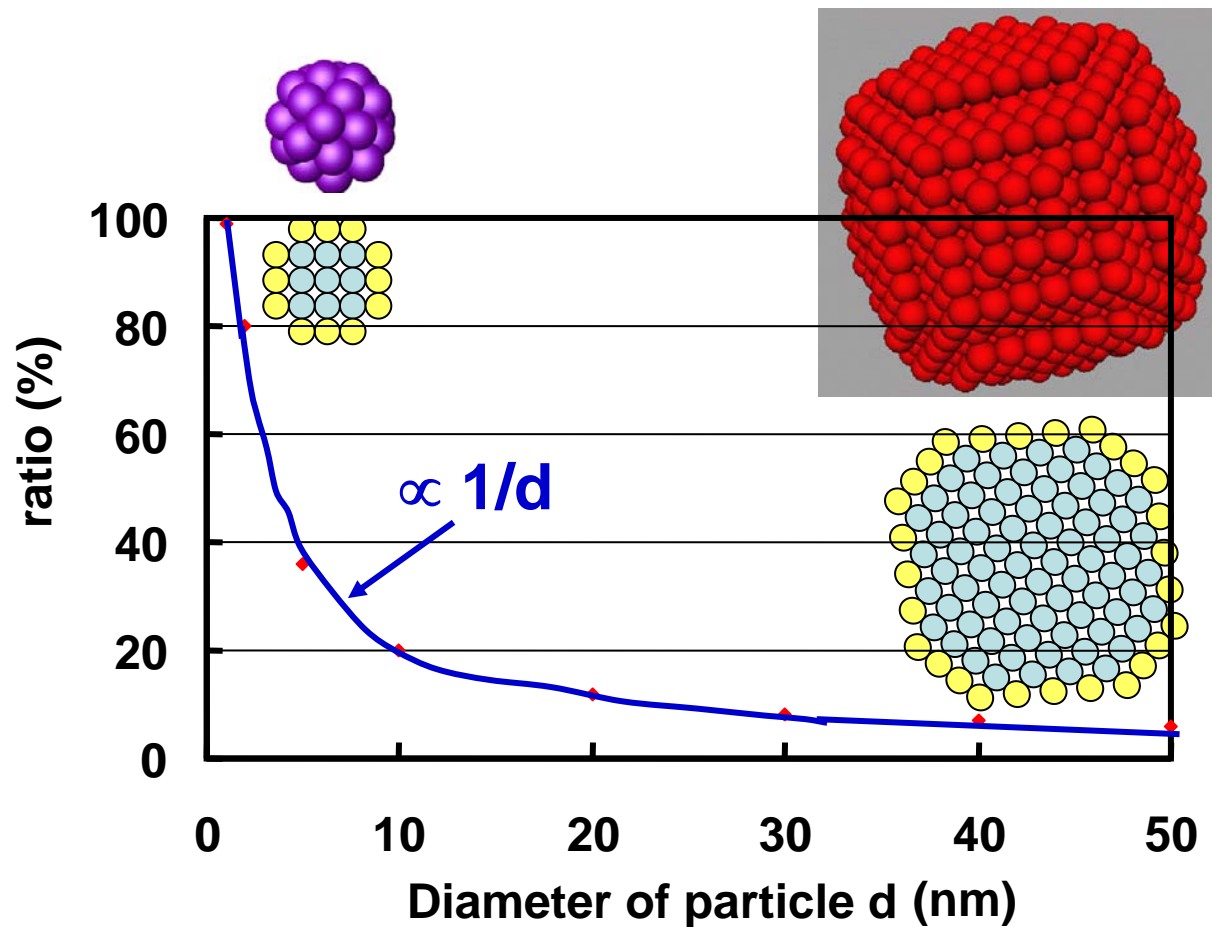


$$\Psi(x) = \begin{cases} \sin(n\pi x/a), & n \text{ even} \\ \cos(n\pi x/a), & n \text{ odd} \end{cases}$$

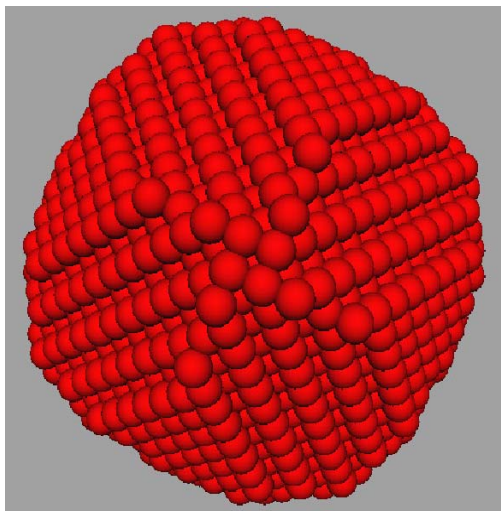
$$E = n^2\pi^2\hbar^2/2ma^2, \quad n = 1, 2, 3, \dots$$



Ratio of surface atoms



Au nanoparticle as an example



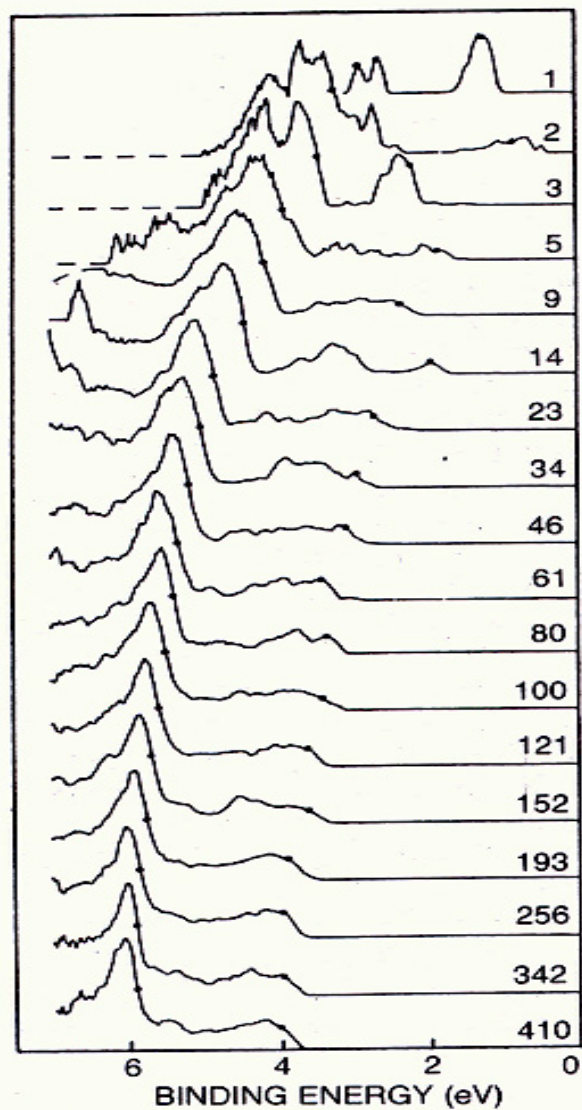
$$E_F = (\hbar^2/2m) (3\pi^2 n)^{2/3}$$

$$g(E_F) = (3/2) (n/E_F)$$

$$\delta = 2/[g(E_F)V] = (4/3) (E_F/N)$$

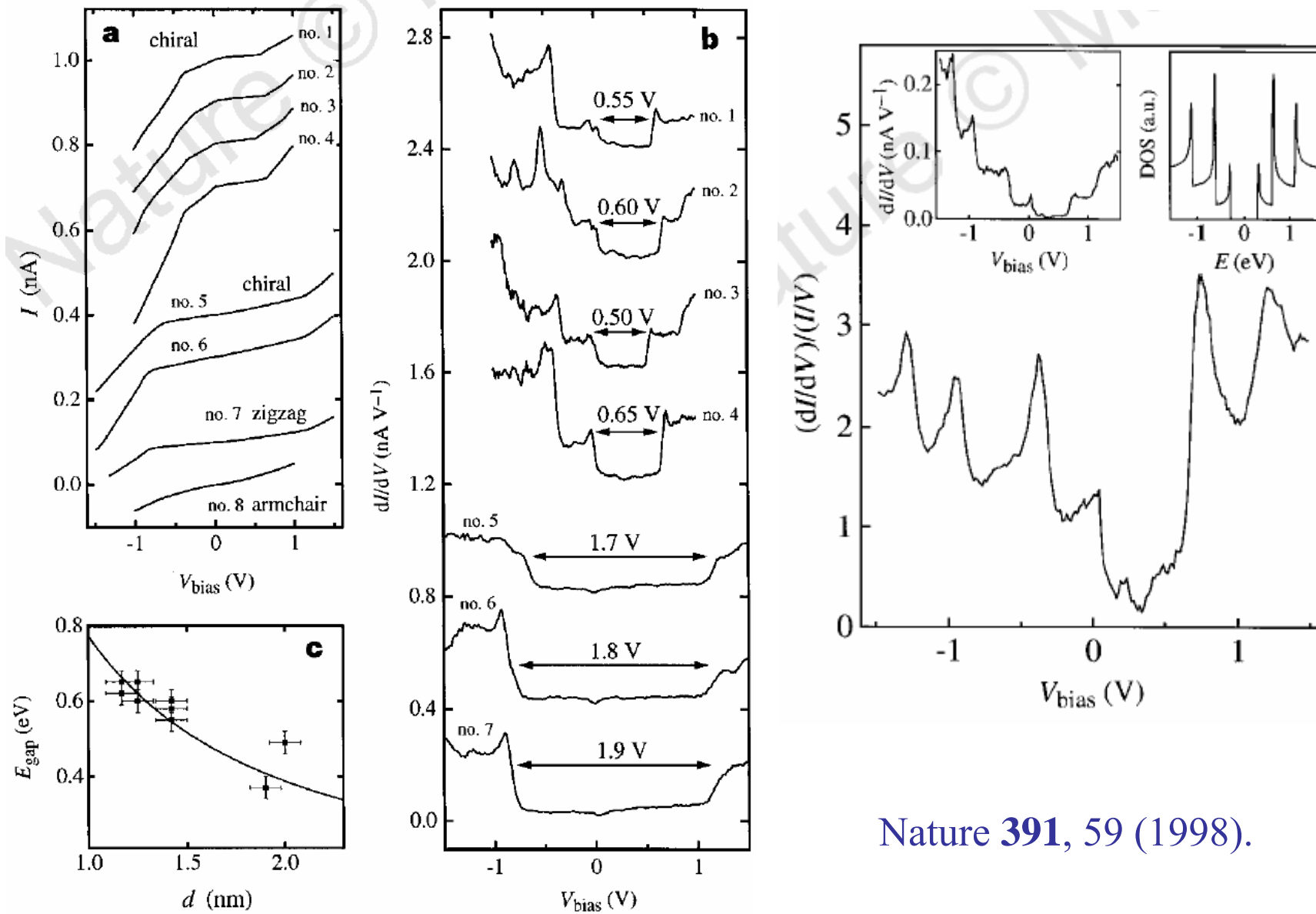
Number of valence electrons (N) contained in the particles is roughly 40,000. Assume the Fermi energy (E_F) is about 7 eV for Au, then

$$\delta \sim 0.22 \text{ meV} \sim 2.5 \text{ K}$$



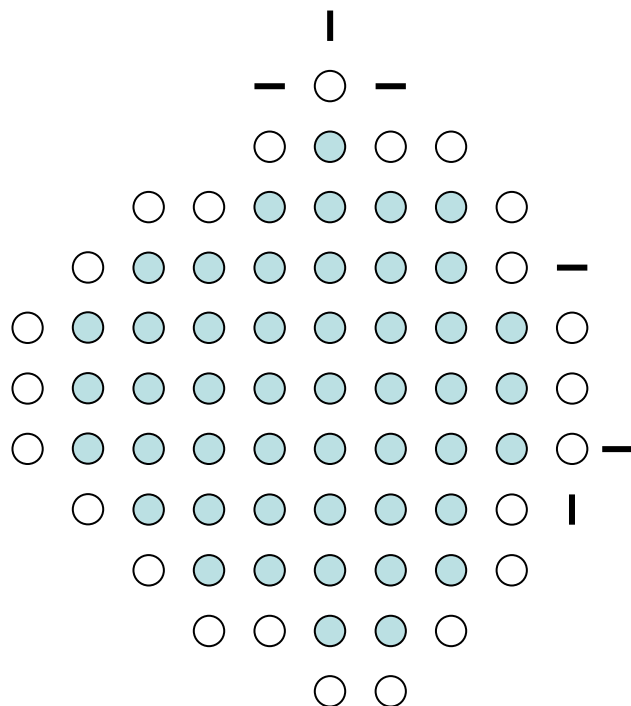
Ultraviolet photoemission spectra of ionized copper clusters Cu_N^- ranging in size from N of 1 to 410 show the energy distribution versus binding energy of photoemitted electrons. These photoemission patterns show the evolution of the 3d band of Cu as a function of cluster size. As the cluster size increases, the electron affinity approaches the value of the bulk metal work function. (Adapted from ref. 10.) **Figure 5**

Electronic Structure of Single-wall Nanotubes



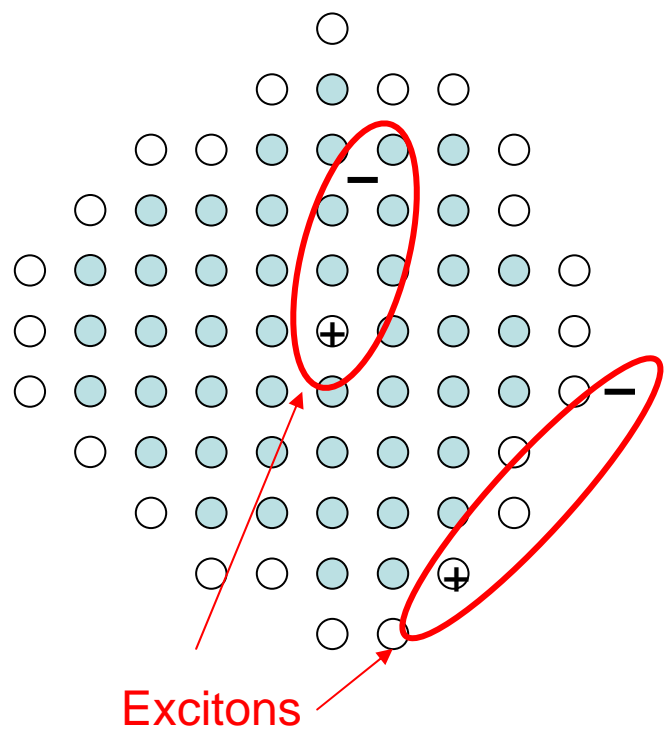
Nature 391, 59 (1998).

Optical properties of nanoparticles (in the infrared range)



- (1) Broad-band absorption:
Due mainly to the increased normal modes at the surface.
- (2) Blue shift:
Due mainly to the bond shortening resulted from surface tension.

Optical properties of nanoparticles (in the visible light range)



(1) Blue shift:

Due mainly to the energy-gap widening because of the size effect.

(2) Red shift:

Bond shortening resulted from surface tension causes more overlap between neighboring electron wavefunctions. Valence bands will be broadened and the gap becomes narrower.

(3) Enhanced exciton absorption:

Due mainly to the increased probability of exciton formation because of the confining effect.

Optical properties

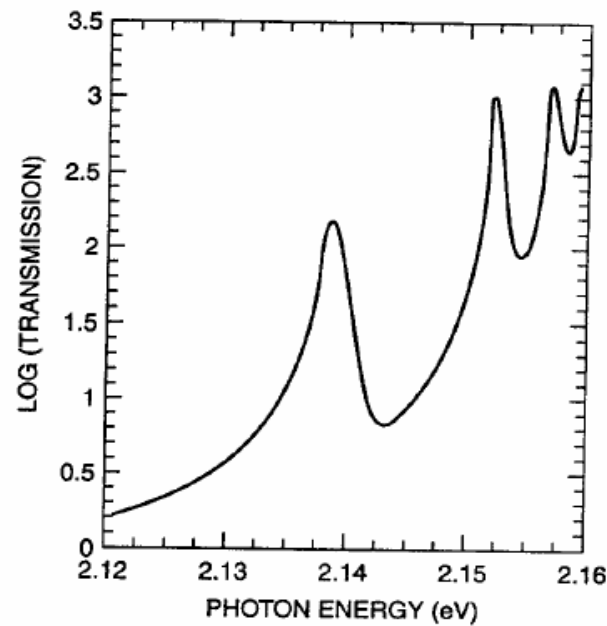


Figure 4.19. Optical absorption spectrum of hydrogen-like transitions of excitons in Cu₂O. [Adapted from P. W. Baumeister, *Phys. Rev.* **121**, 359 (1961).]

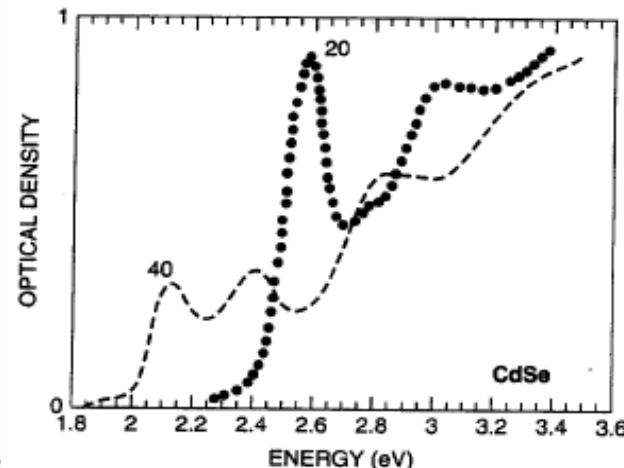
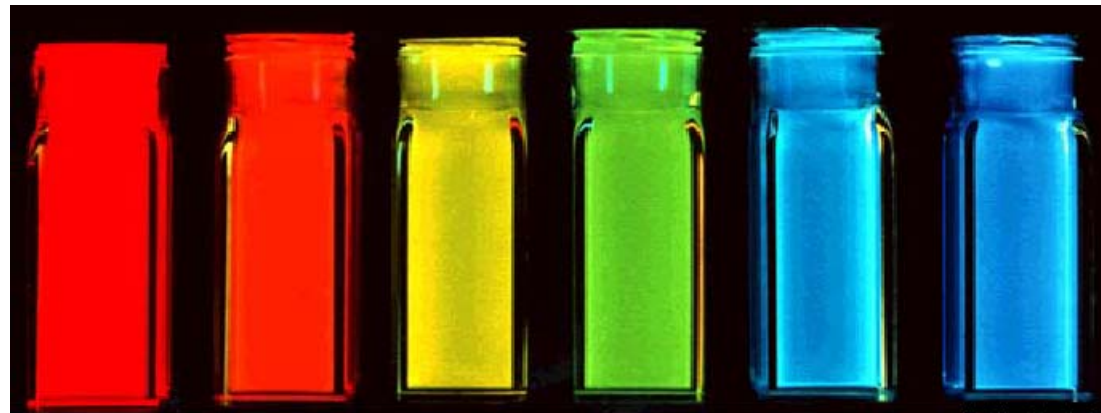
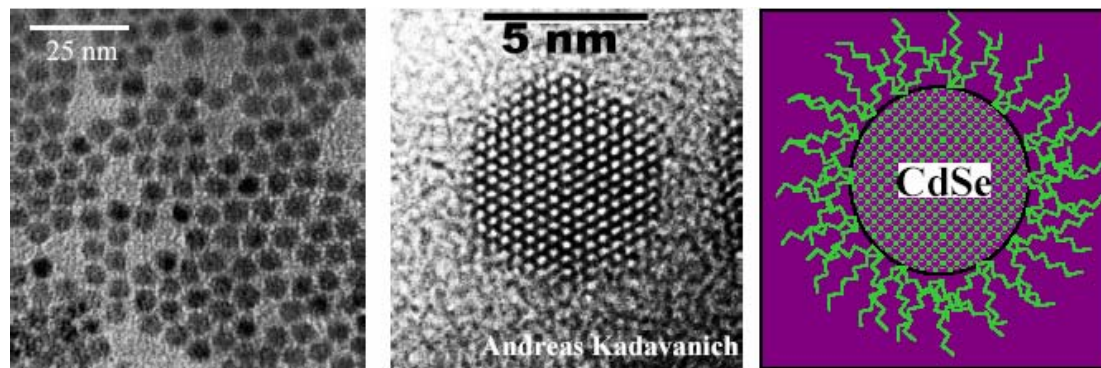
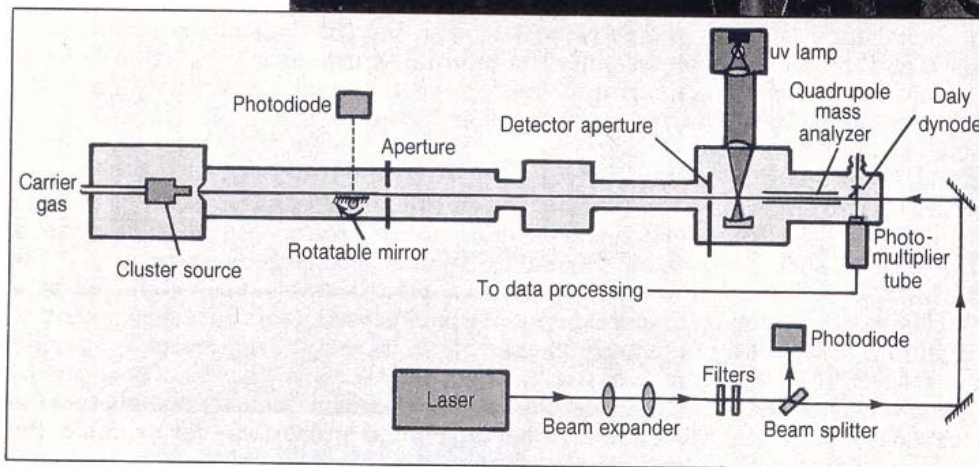
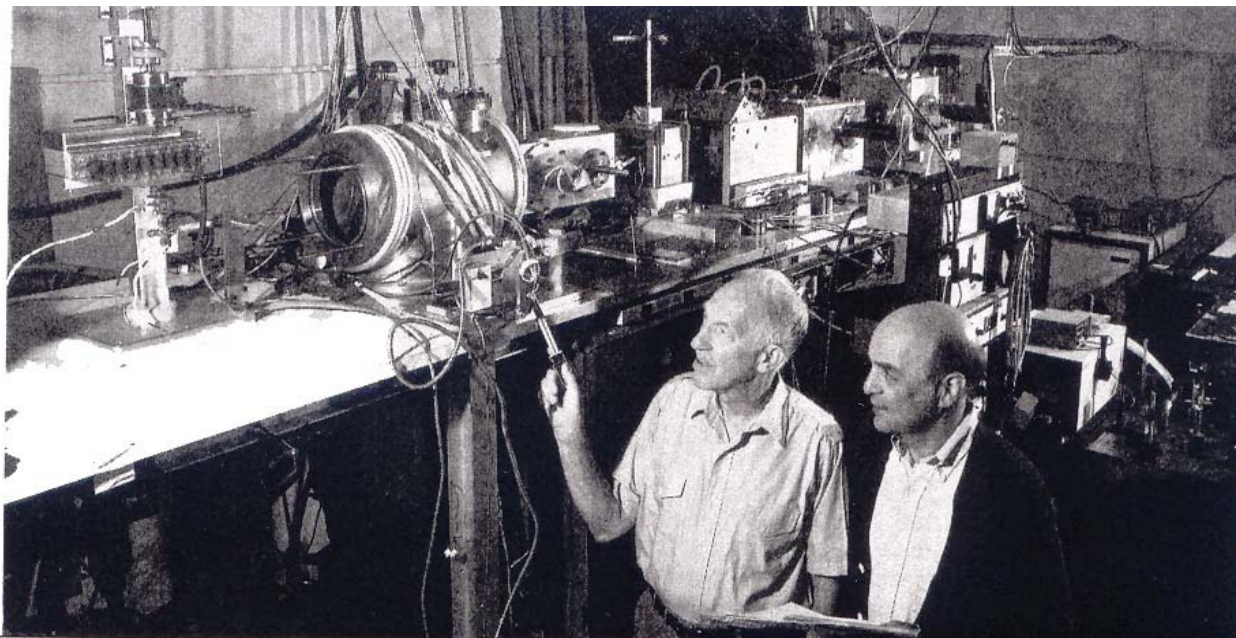


Figure 4.20. Optical absorption spectrum of CdSe for two nanoparticles having sizes 20 Å and 40 Å, respectively. [Adapted from D. M. Mittleman, *Phys. Rev. B* **49**, 14435 (1994).]

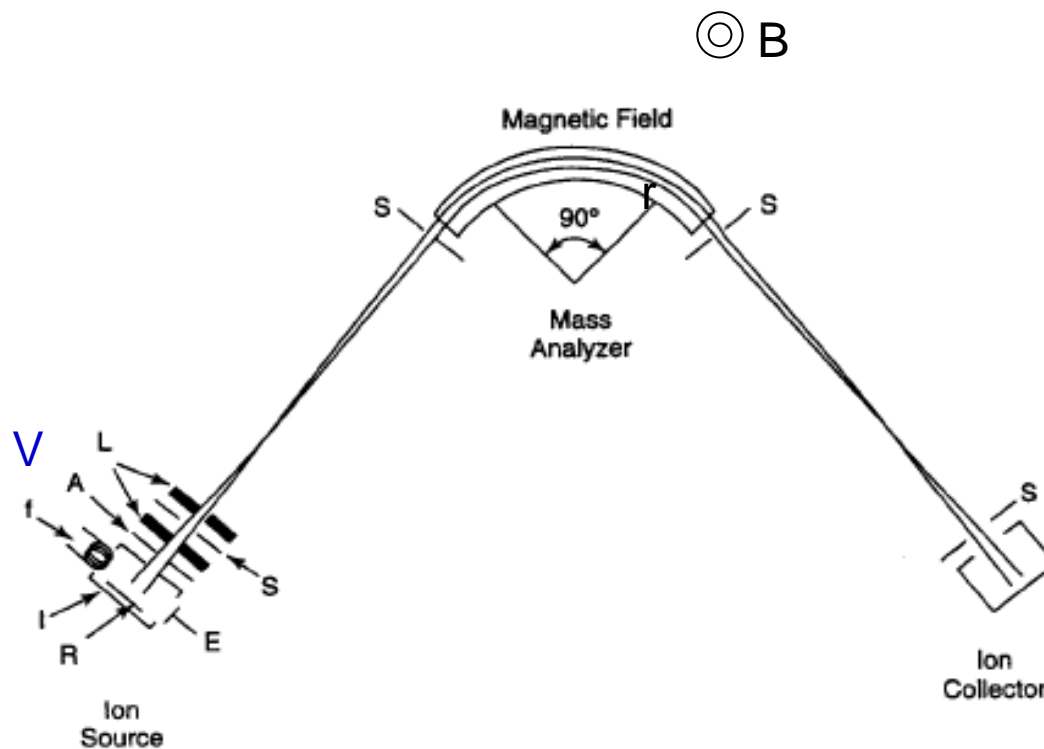
Semiconductor quantum dots



(Reproduced from Quantum Dot Co.)



Mass Analyzer

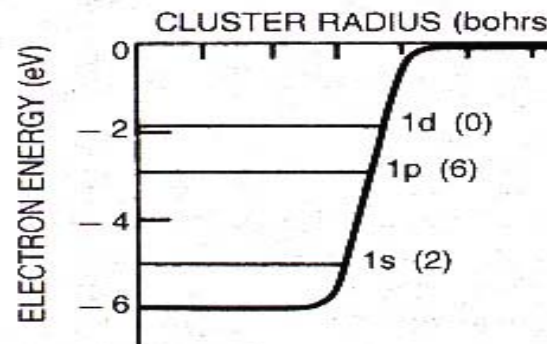


$$qV = \frac{1}{2} mv^2$$

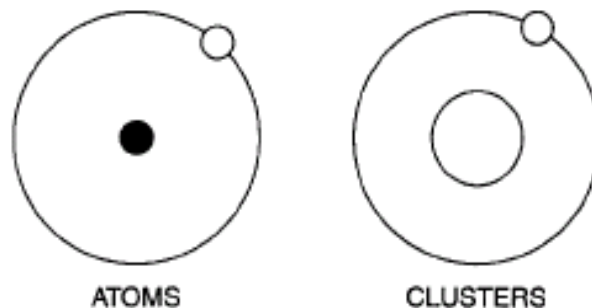
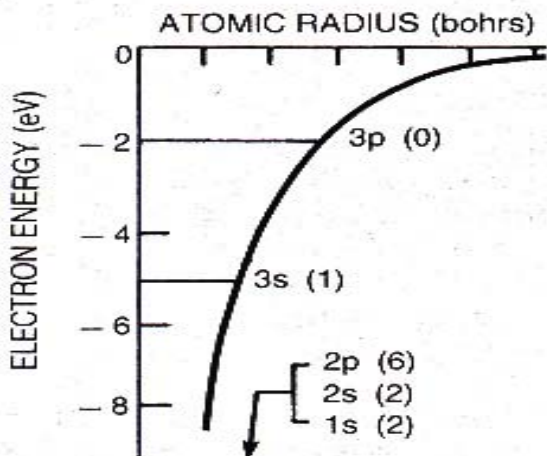
$$F = qvB = mv^2/r$$

$$m/q = \frac{1}{2} B^2 r^2/V$$

Figure 3.8. Sketch of a mass spectrometer utilizing a 90° magnetic field mass analyzer, showing details of the ion source: A—accelerator or extractor plate, E—electron trap, f—filament, I—ionization chamber, L—focusing lenses, R—repeller, S—slits. The magnetic field of the mass analyzer is perpendicular to the plane of the page.

a**c**

JELLIUM MODEL OF CLUSTERS

**b**

(a)

(b)

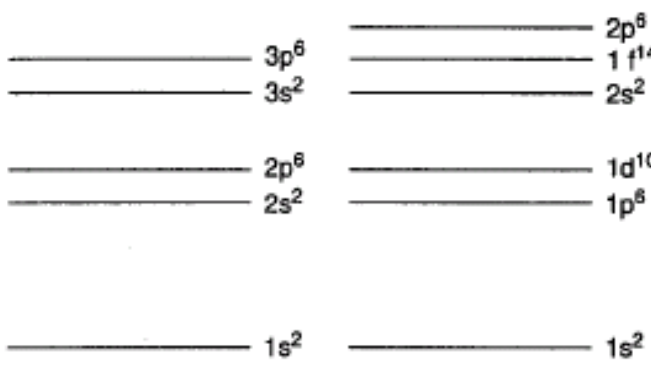
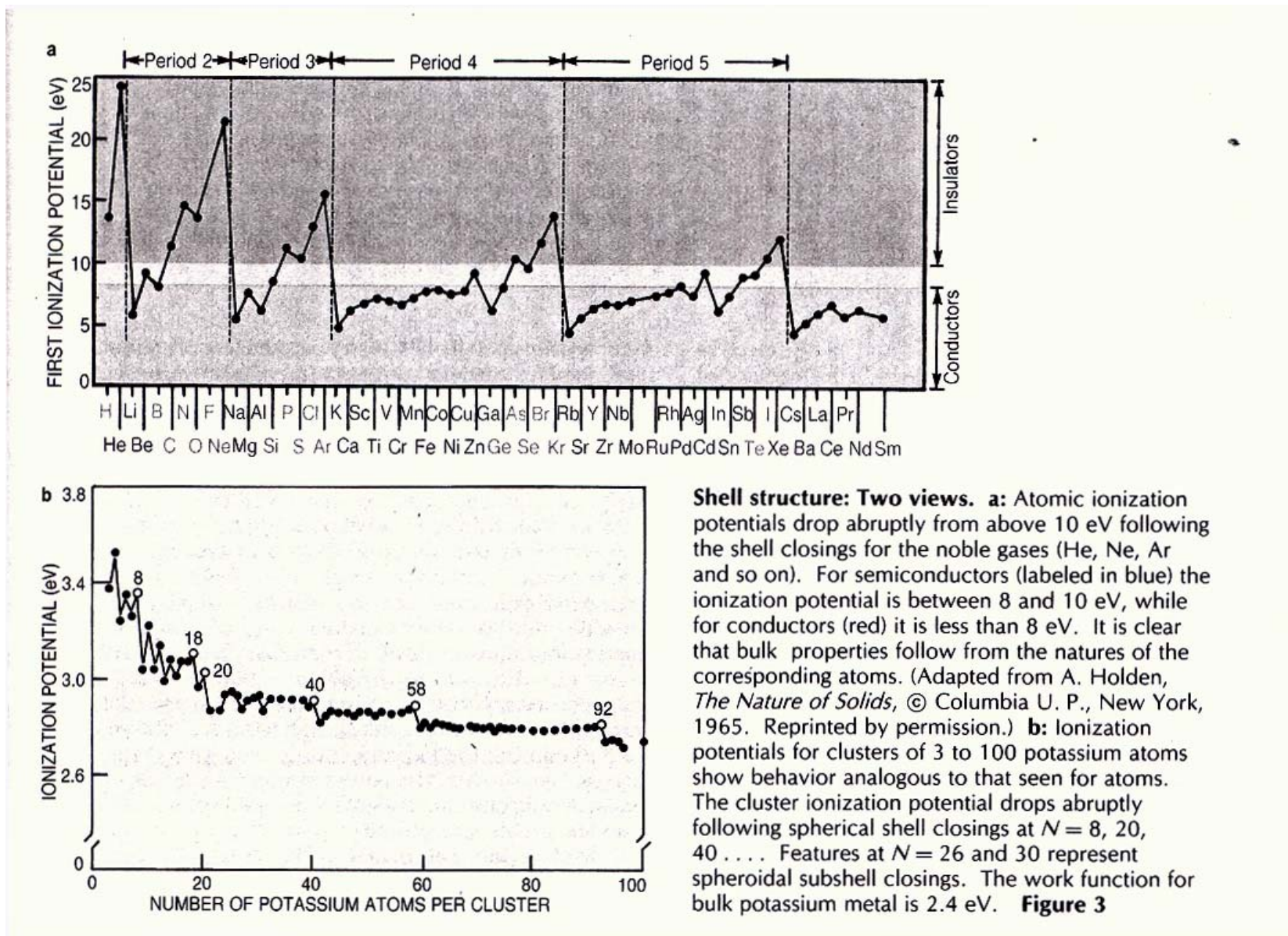
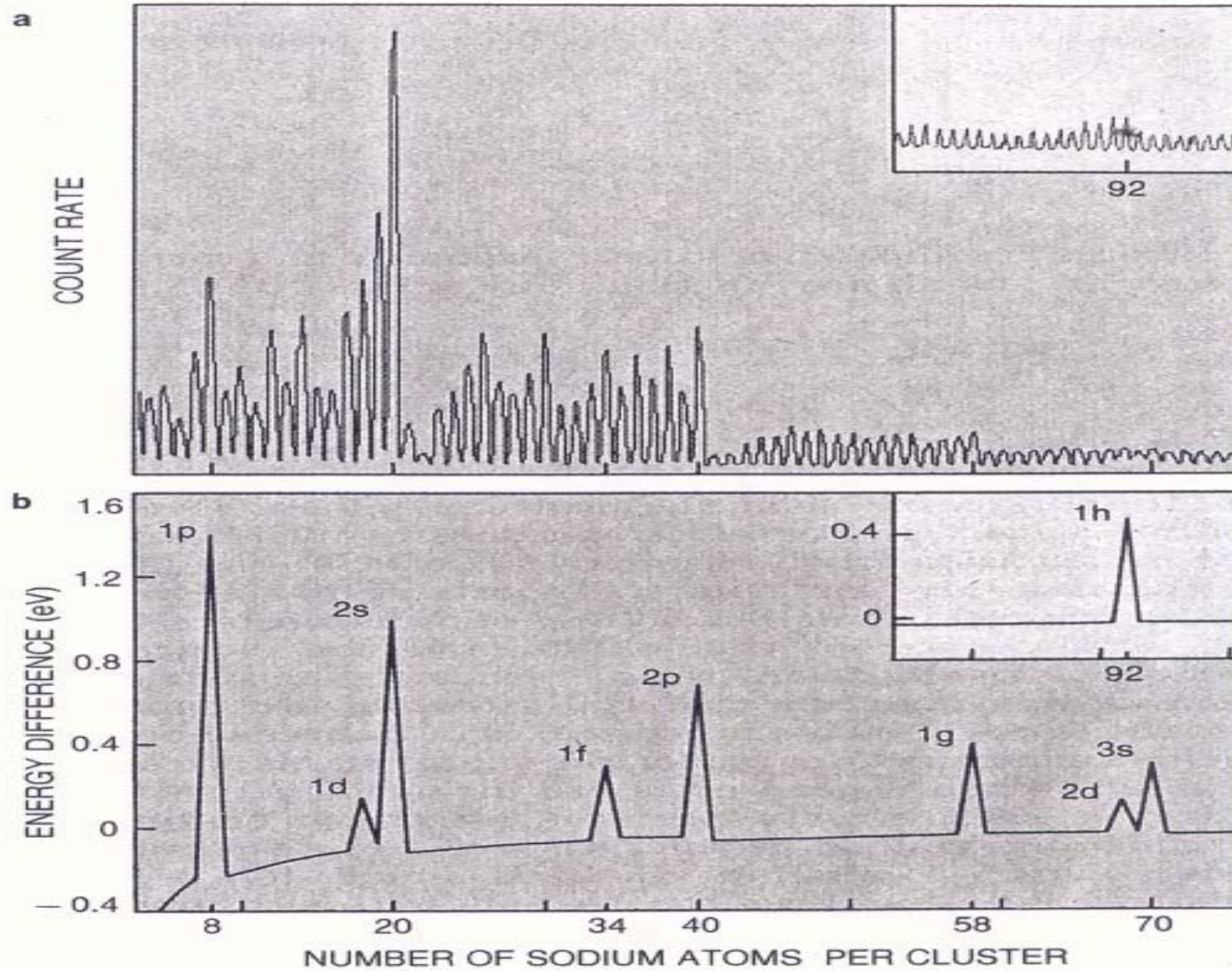


Figure 4.5. A comparison of the energy levels of the hydrogen atom and those of the jellium model of a cluster. The electronic magic numbers of the atoms are 2, 10, 18, and 36 for He, Ne, Ar, and Kr, respectively (the Kr energy levels are not shown on the figure) and 2, 18, and 40 for the clusters. [Adapted from B. K. Rao et al., *J. Cluster Sci.* **10**, 477 (1999).]





Reactivity of nanoclusters

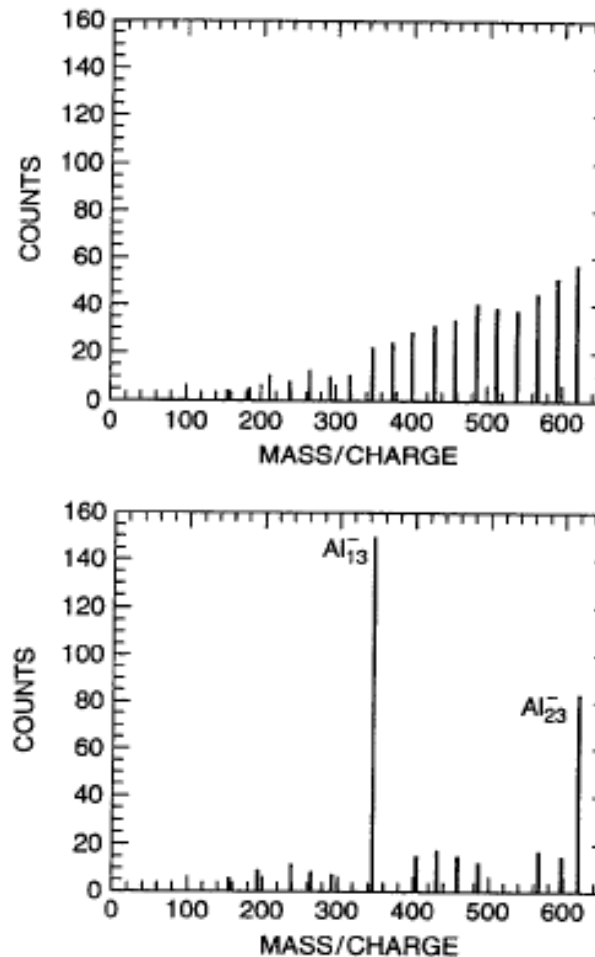


Figure 4.13. Mass spectrum of Al nanoparticles before (top) and after (bottom) exposure to oxygen gas. [Adapted from R. E. Leuchtner et al., *J. Chem. Phys.*, **91**, 2753 (1989).]

Magic clusters

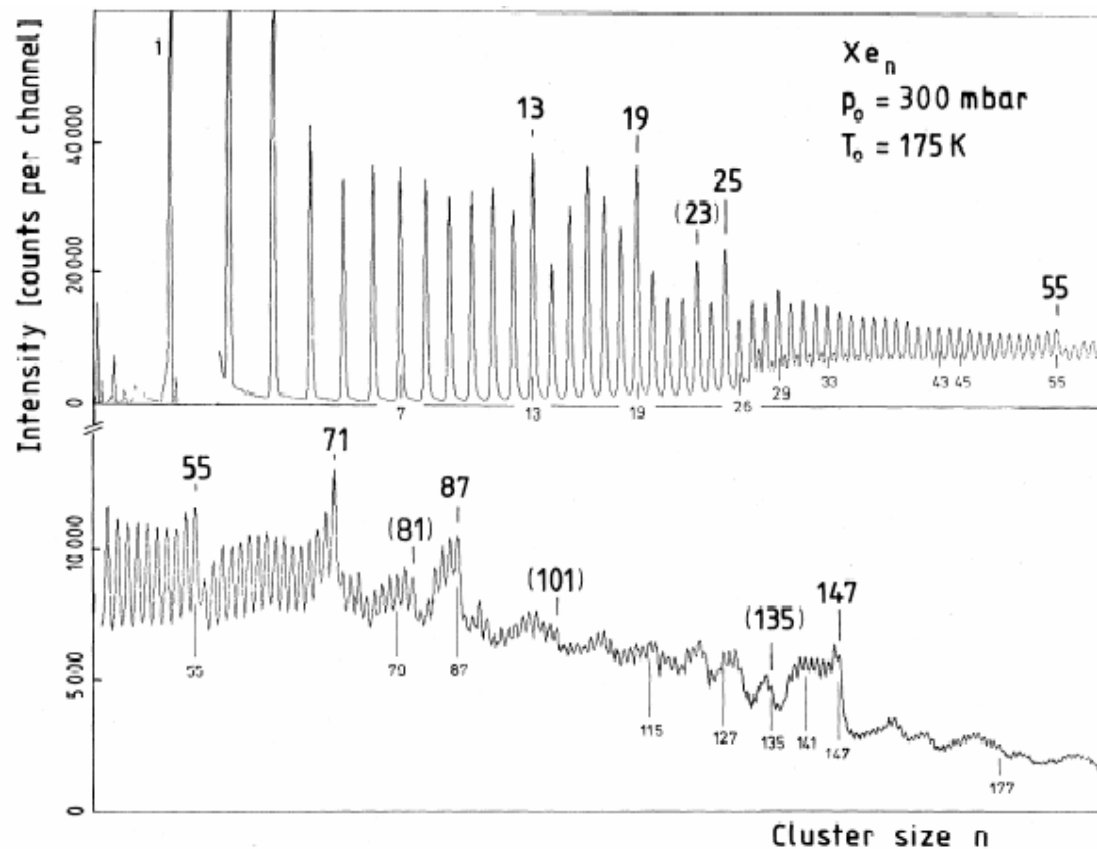
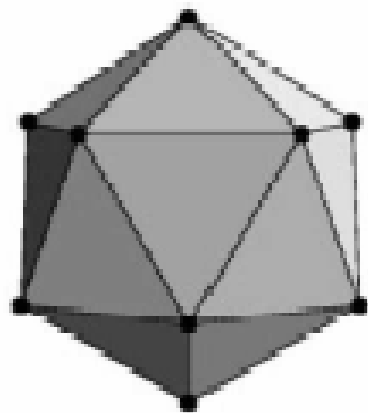


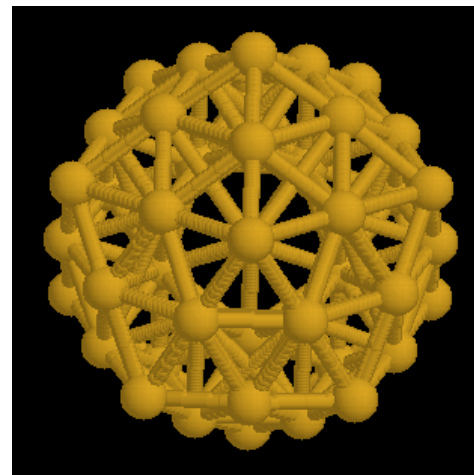
FIG. 1. Mass spectrum of xenon clusters. Observed magic numbers are marked in boldface; brackets are used for numbers with less pronounced effects. Numbers below the curve indicate predictions or distinguished sphere packings.

Mackay icosahedra

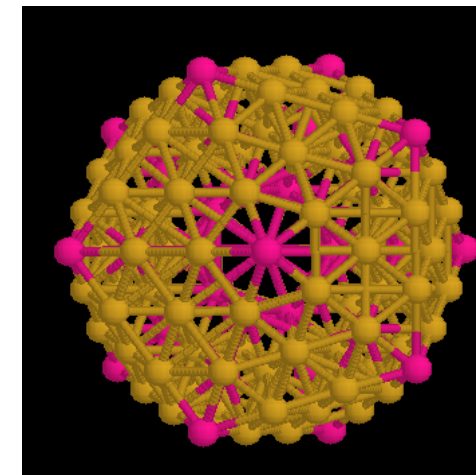


$P = 1$

20 fcc(111) faces



$P = 2$



$P = 3$

Shell model

$$N = 1 + \sum (10p^2 + 2)$$

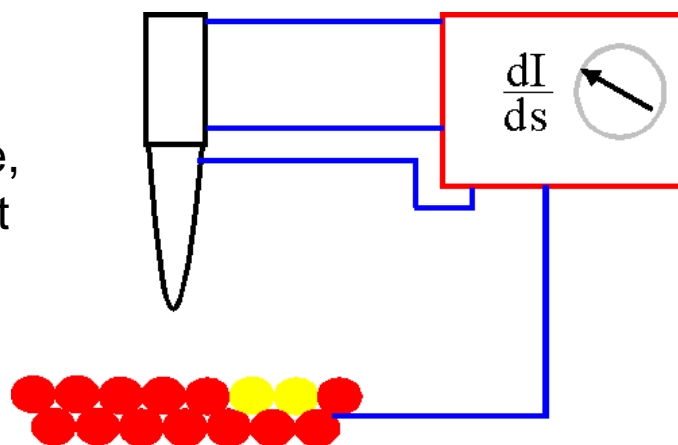
Scanning Tunneling Spectroscopy

1. Barrier Height Imaging

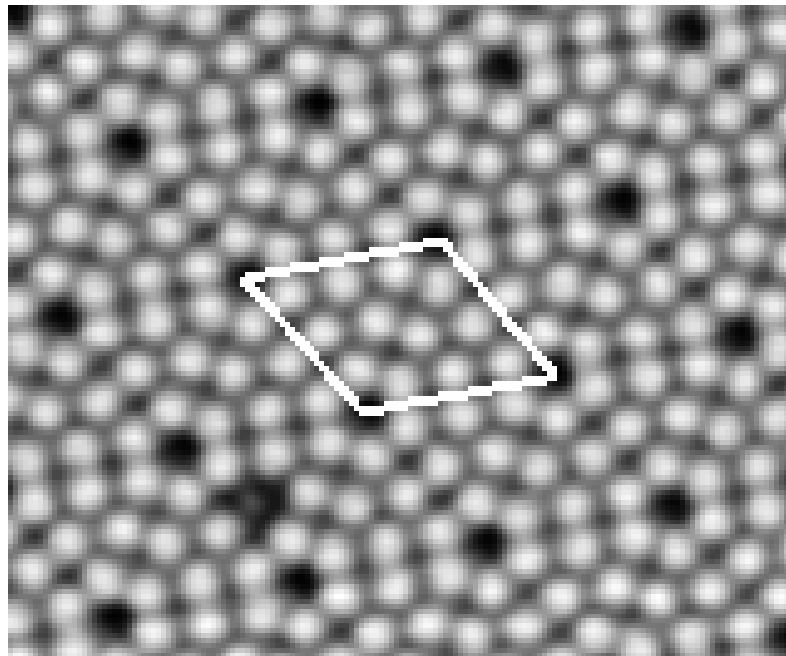
Up to now homogeneous surfaces were considered. If there is an inhomogeneous compound in the surface the work function will be inhomogeneous as well. This alters the local barrier height. Differentiation of tunneling current yields

$$\frac{d(\ln I)}{ds} \propto \sqrt{\Phi}$$

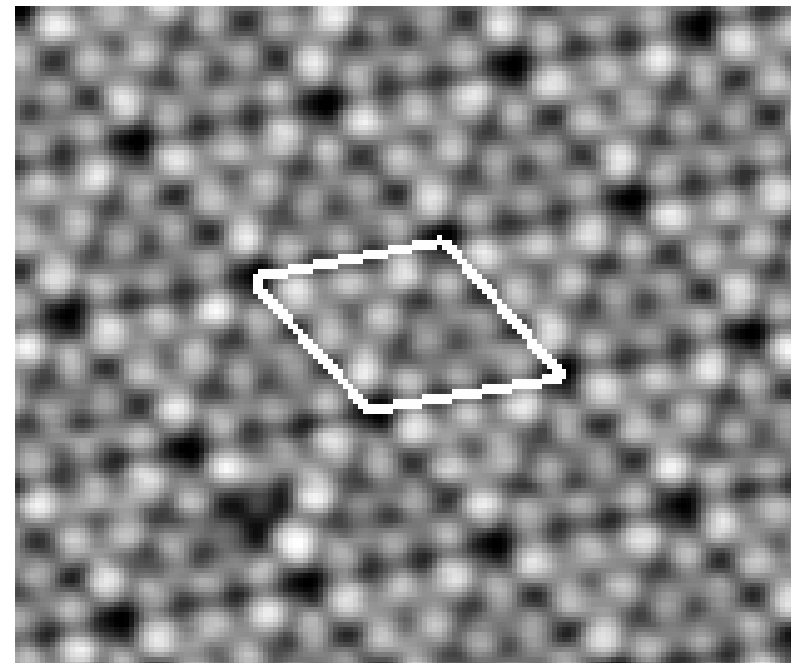
Thus the work function can directly be measured by varying the tip-sample distance, which can be done by modulating the current with the feedback turned on.



STM Images of Si(111)-(7×7)



Empty-state image

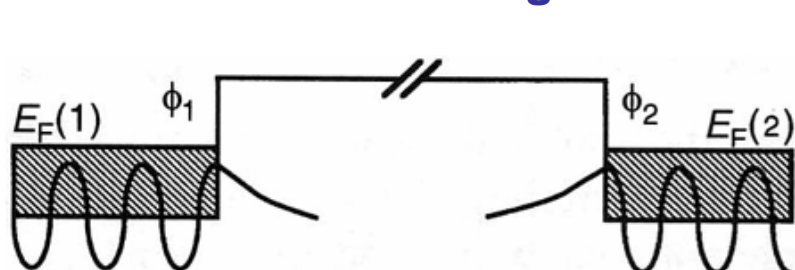


Filled-state image

Electronic Structures at Surfaces

Empty-State Imaging

Not Tunneling



$E_F(1)$

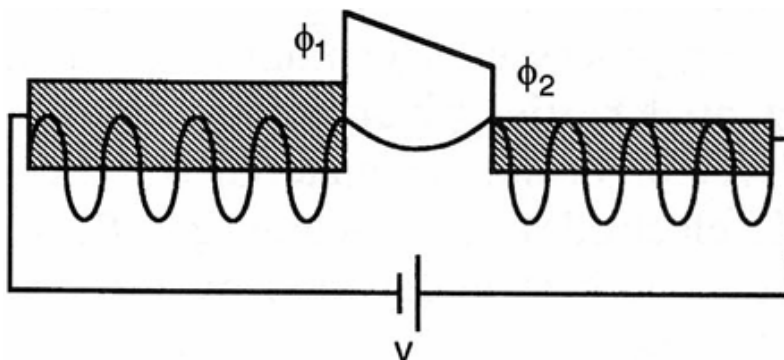
ϕ_2

$E_F(2)$

Tip

Sample

Tunneling



Filled-State Imaging

$E_F(1)$

Tip

$E_F(2)$

$\phi(2)$

Sample

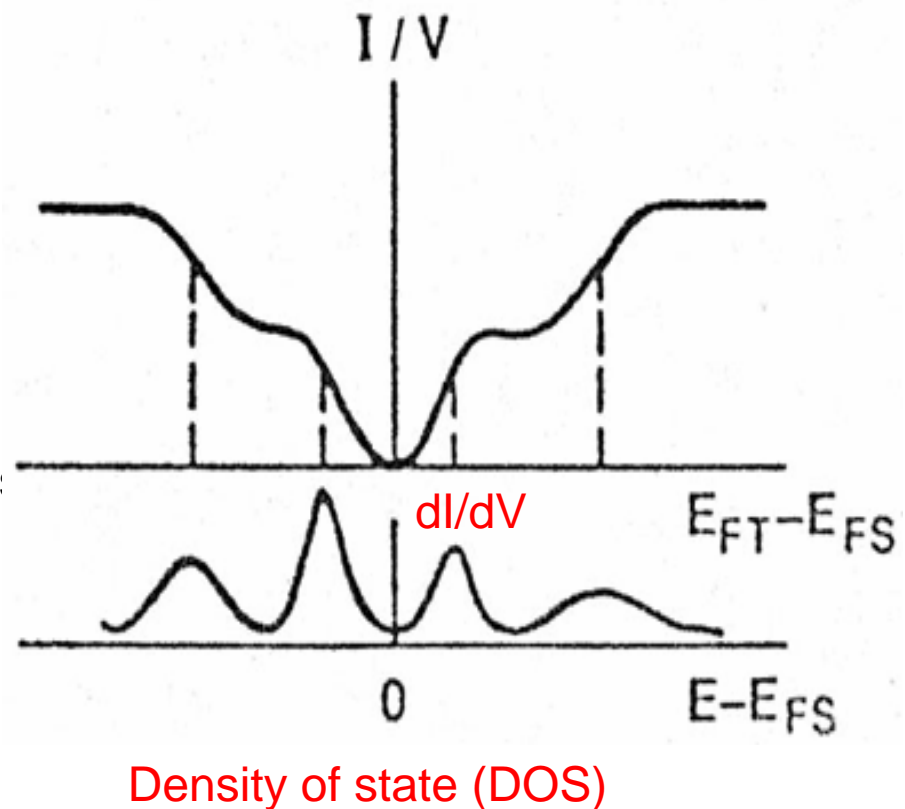
2. dI/dV imaging

If the matrix element and the density of states of the tip is nearly constant, the tunneling current can be estimated to

$$I \propto \int_0^{\infty} \rho_{sa} (E_F - eV + \varepsilon) d\varepsilon$$

Differentiation yields the density of states

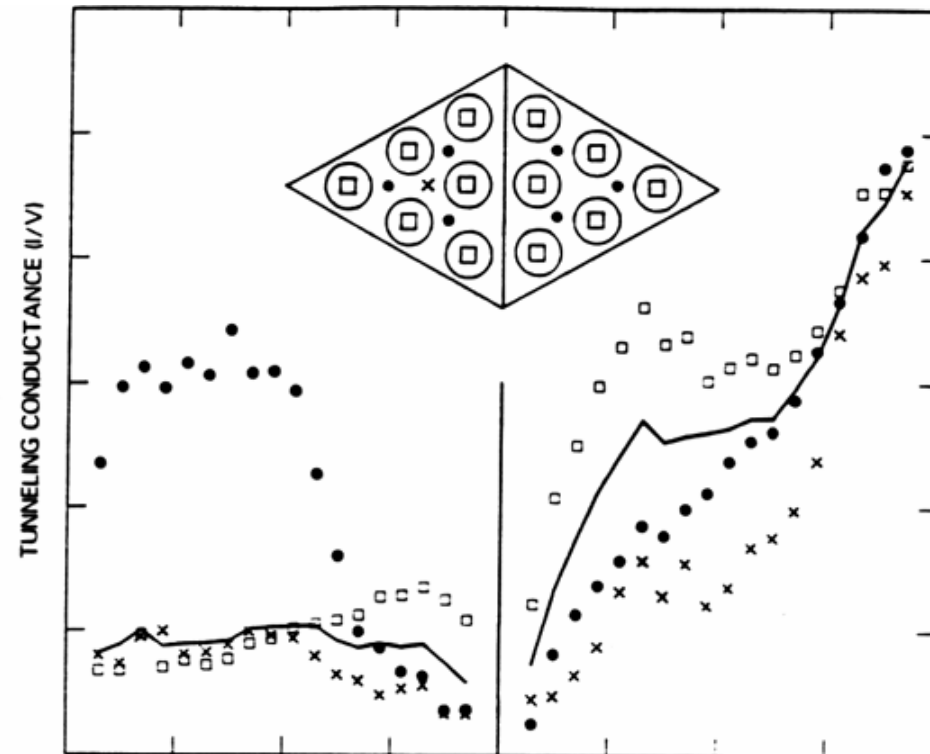
$$\frac{dI}{dV} \propto \rho_{sa} (E_F - eV)$$



The mapping of surface density of states can be deduced by

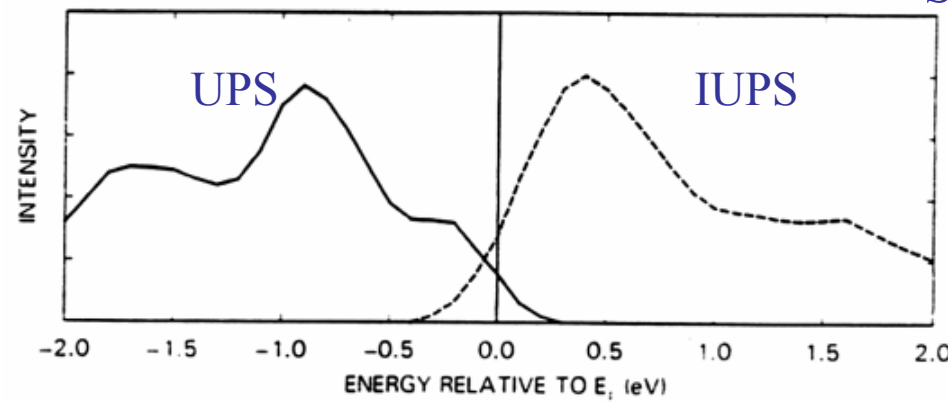
- Modulation of the bias voltage (dI/dV imaging):
The tip is scanned in the constant current mode to give a constant distance to the sample. A dither voltage of $\sim 1\text{ k Hz}$ is added to the bias voltage while the feedback loop remains active. A lock-in technique is employed to obtain the current change at the dither frequency.
- Current-Imaging Tunneling Spectroscopy (CITS): The tip is scanned in the constant current mode to give a constant distance to the sample. At each point the feedback loop is disabled and a current-voltage curve (I-V curve) is recorded.

STS of Si(111)-(7x7)



(a)

Science 234, 304 (1986).

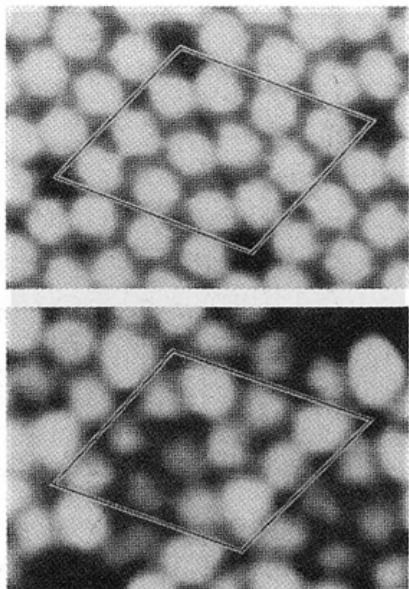


(b)

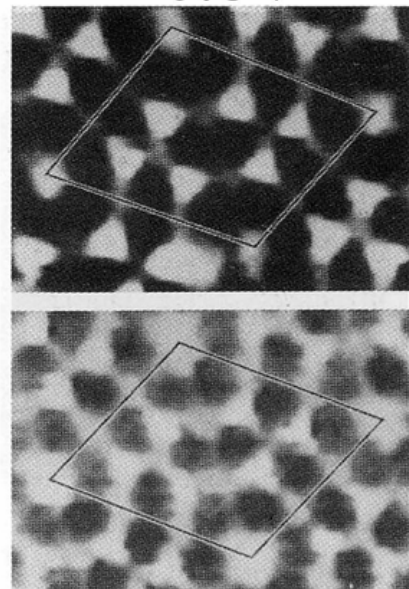
STS of Si(111)-(7x7)

topograph

+2V

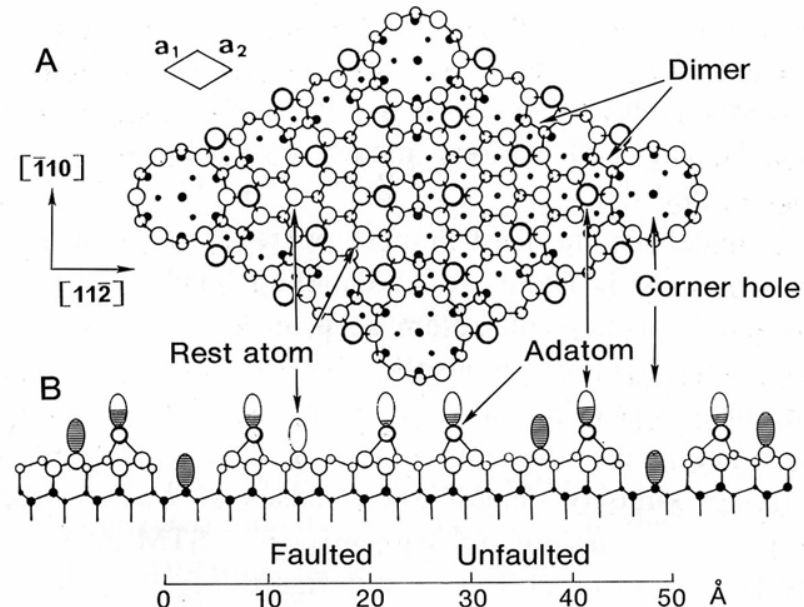


-0.8V



-0.35V

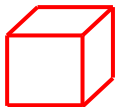
-1.8V



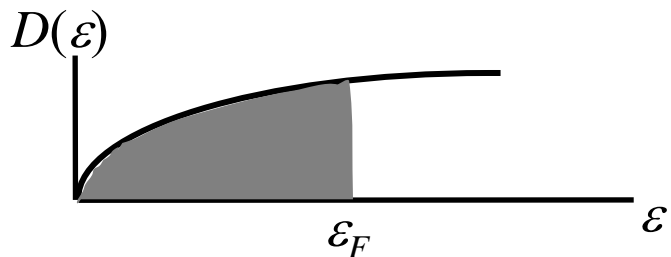
1. Science **234**, 304-309 (1986).
2. Phys. Rev. Lett. **56**, 1972-1975 (1986).

Density of states of various dimensions

3D



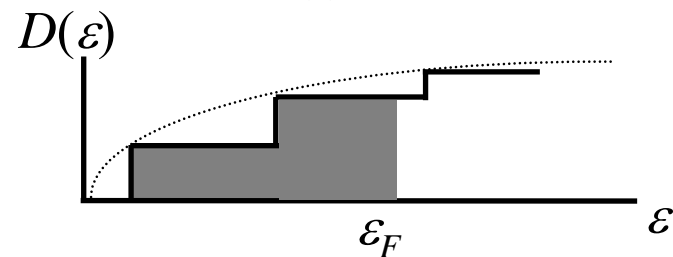
$$D(\varepsilon) \sim \varepsilon^{1/2}$$



2D



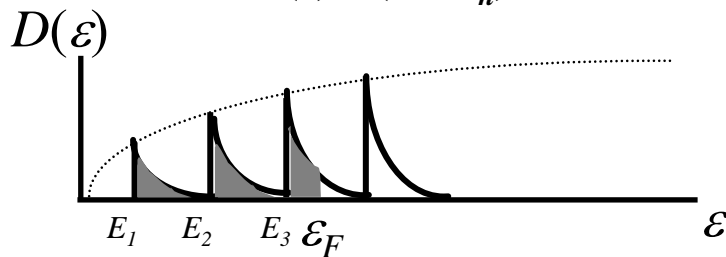
$$D(\varepsilon) = m^* / \pi \hbar^2$$



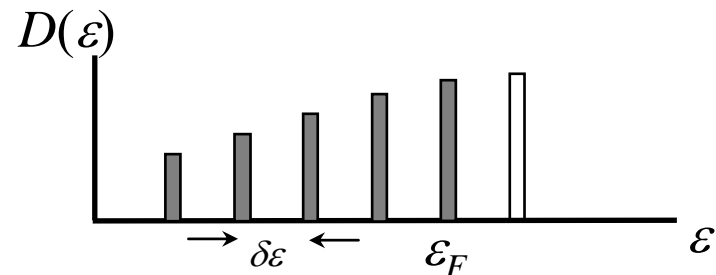
1D



$$D(\varepsilon) \sim (\varepsilon - E_n)^{-1/2}$$

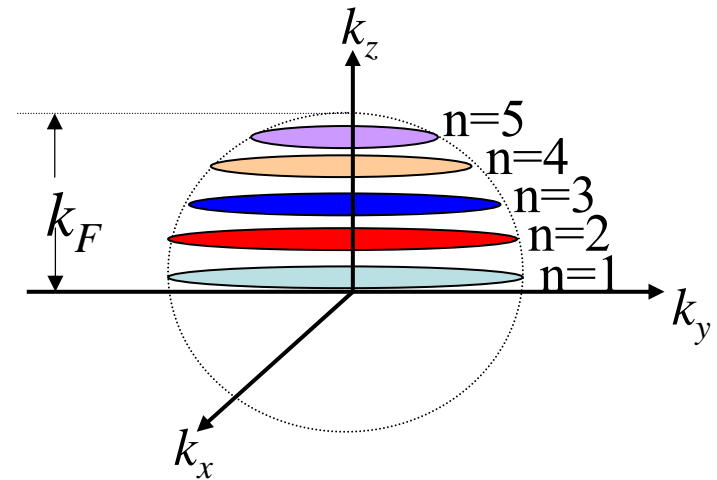
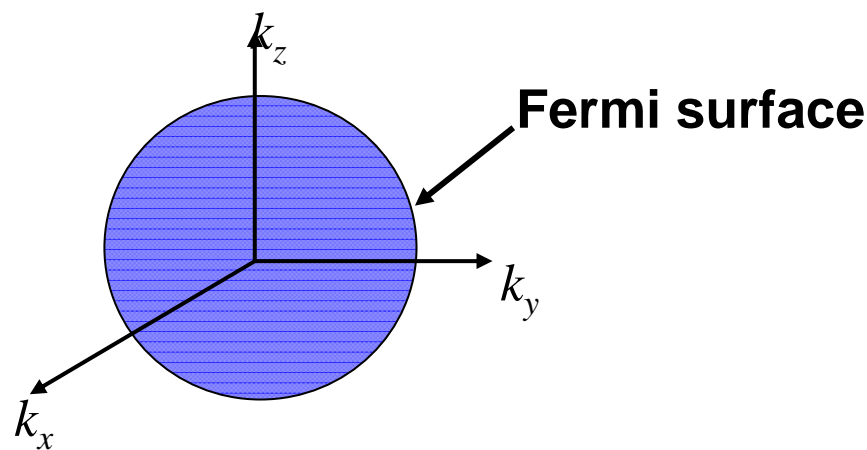
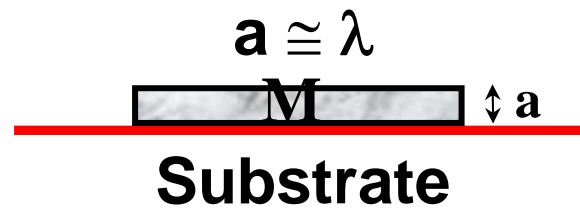
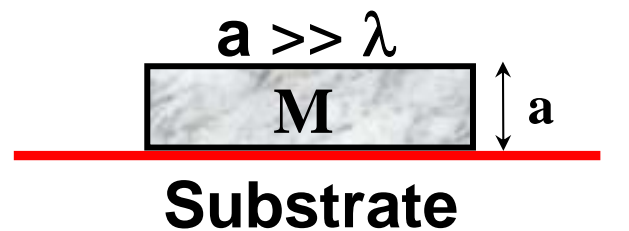


0D



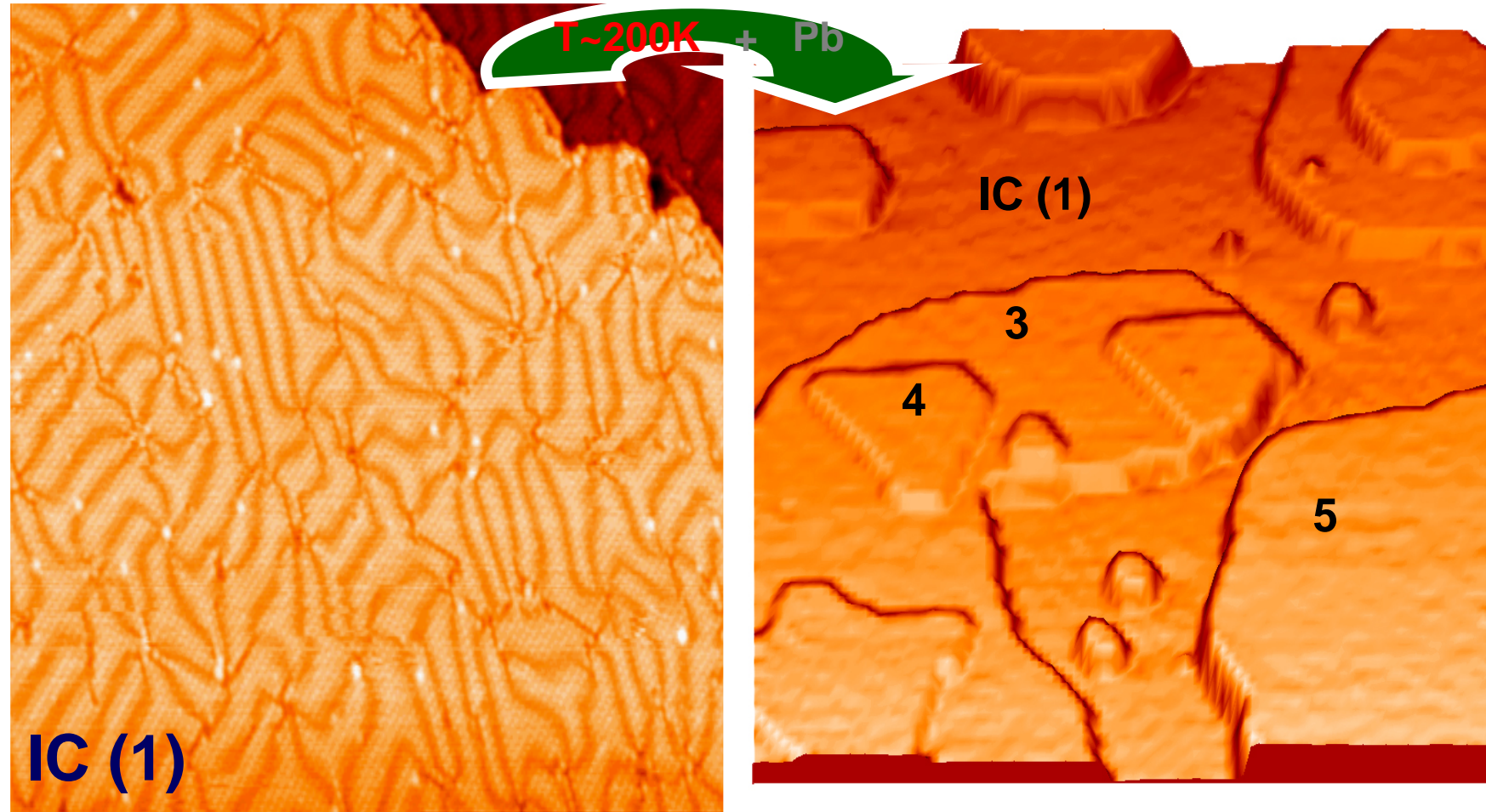
Quantum size effect

λ = de Broglie wavelength of electron
 a = thickness of metal film



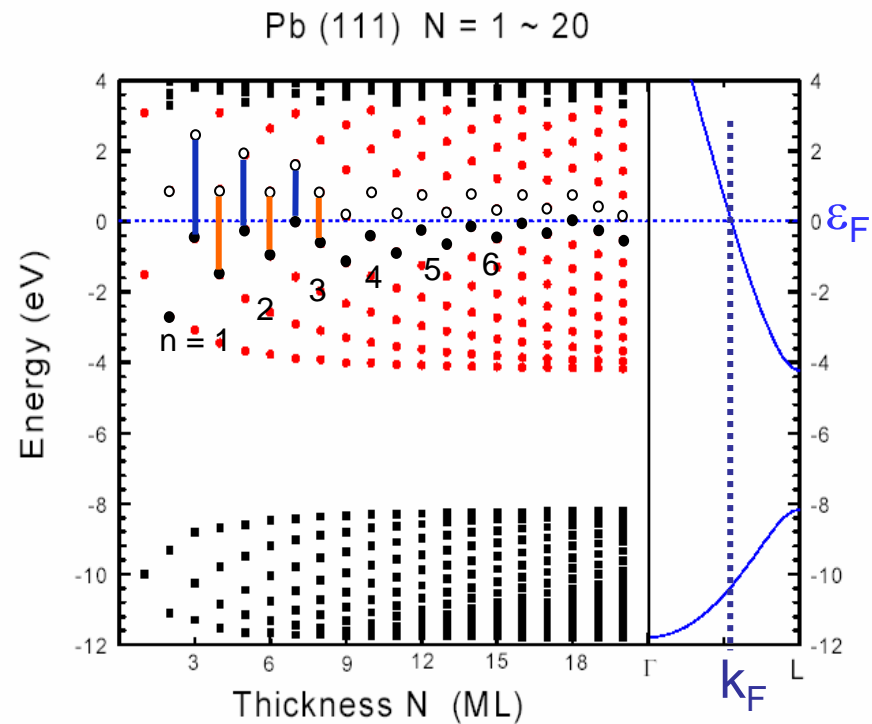
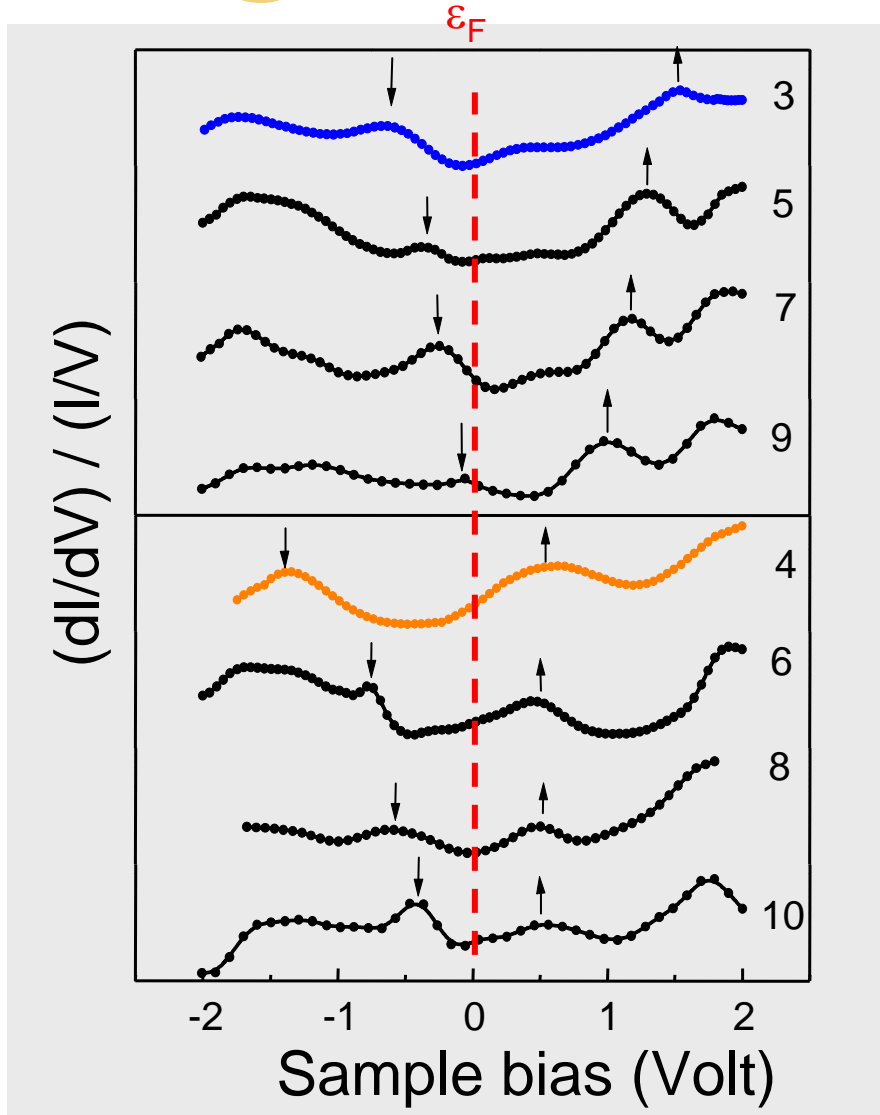


Pb islands on the IC Pb/Si(111)





Spectra for Pb Films



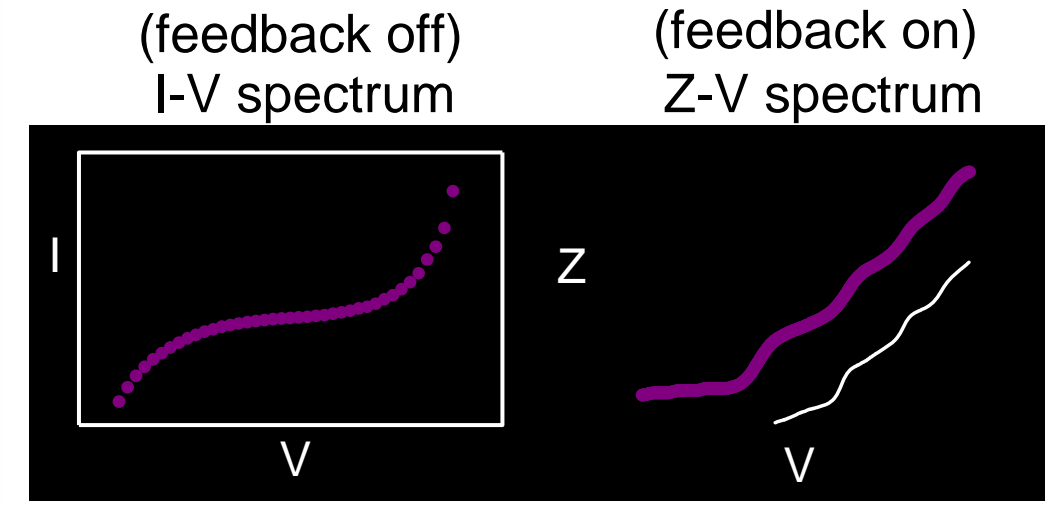
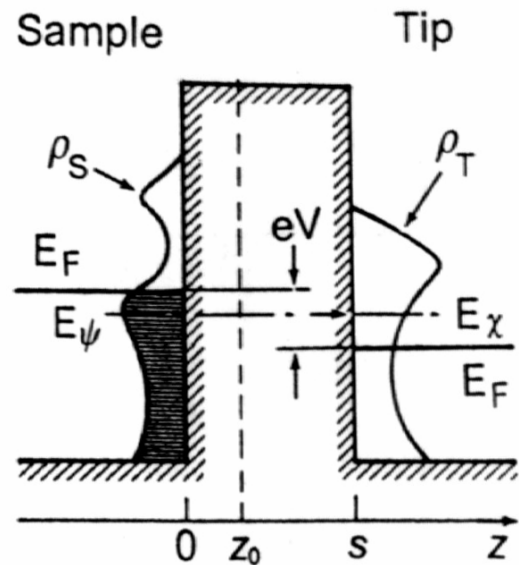
C.M. Wei and M.Y. Chou

$$d_0 = 2.85 \text{ \AA} \quad \lambda_F = 3.94 \text{ \AA}$$

$$2d_0 \approx 3(\lambda_F/2)$$

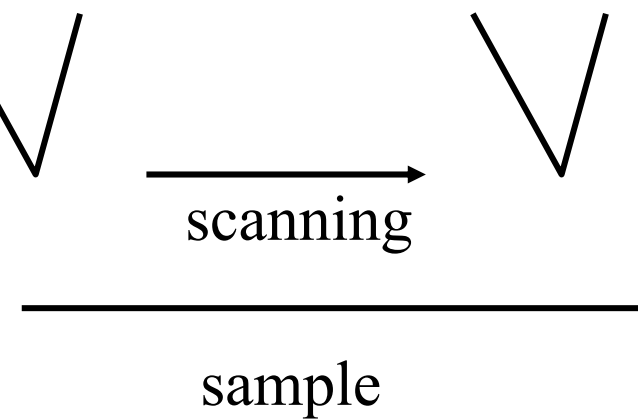


Scanning Tunneling Spectroscopy (STS)



$$I \propto \int_0^{eV} \rho_s(E_F - eV + \varepsilon) \rho_T(E_F + \varepsilon) d\varepsilon$$

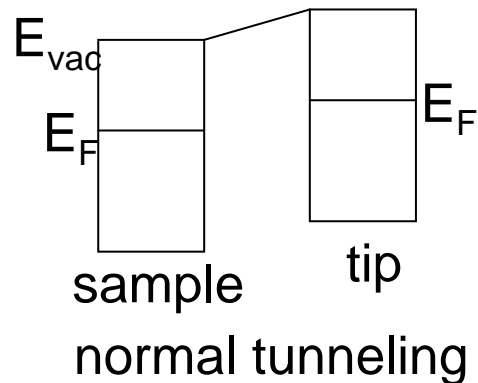
$$\rho_T \text{ is constant} \Rightarrow dI/dV \propto \rho_s(E_F - eV)$$



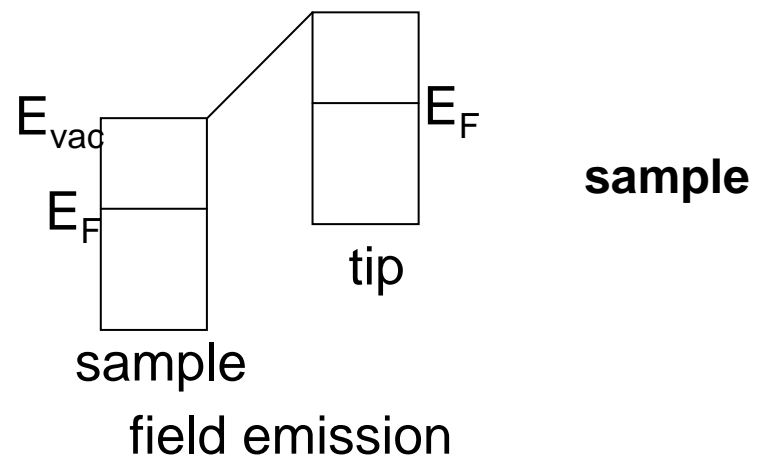


Gundlach Oscillation in STS

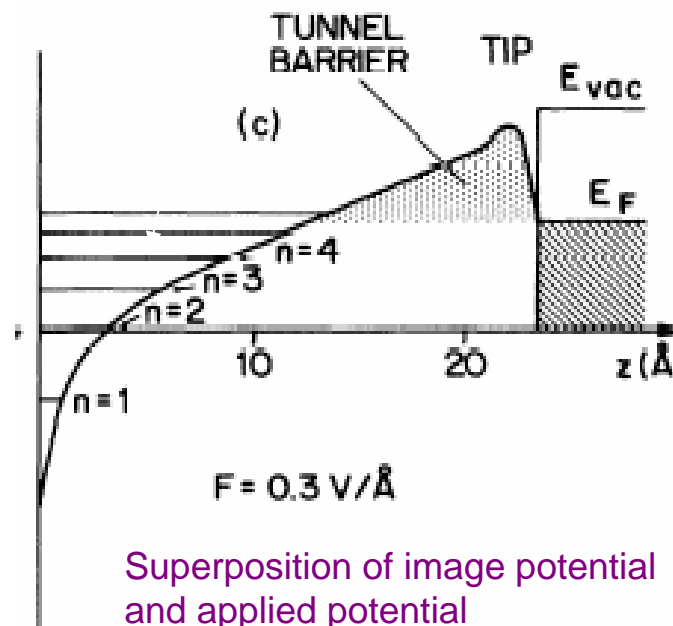
E_F of tip < E_{vac} of sample



E_F of tip > E_{vac} of sample

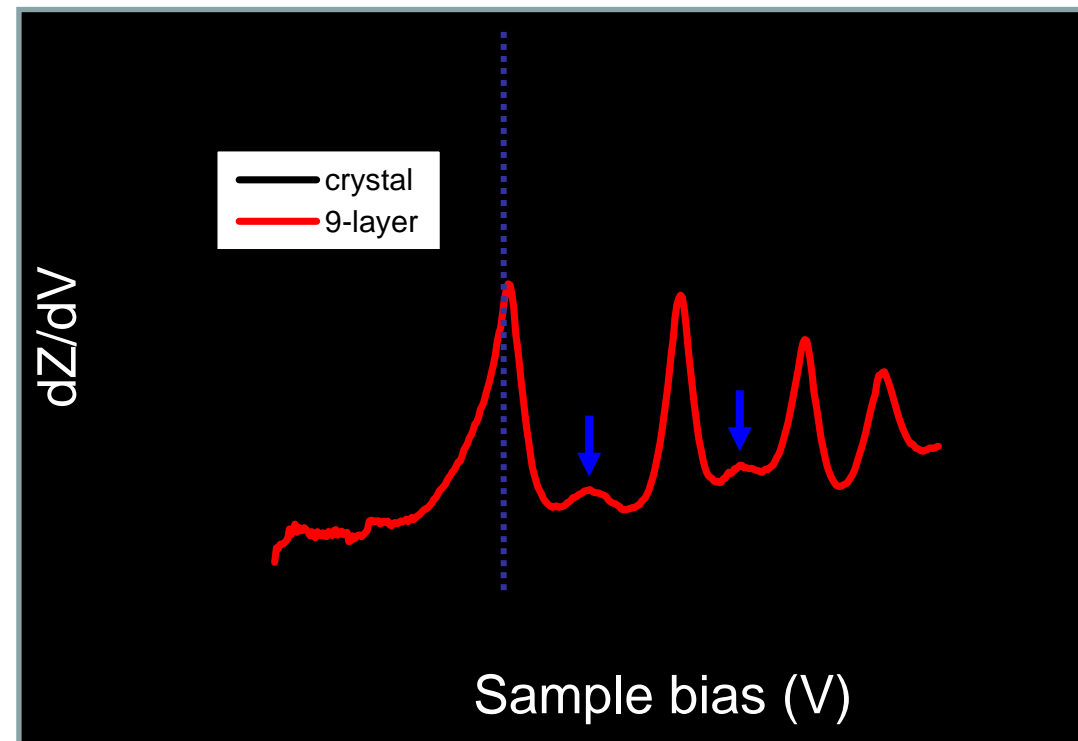
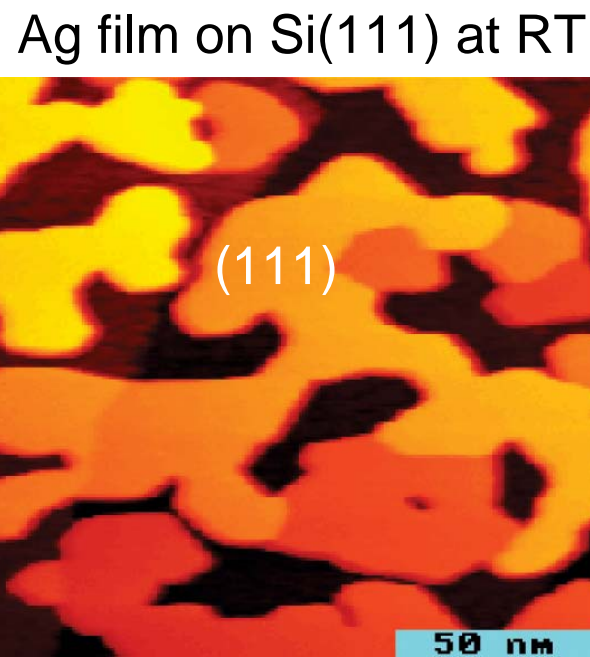


Standing-wave states
in tunneling gap





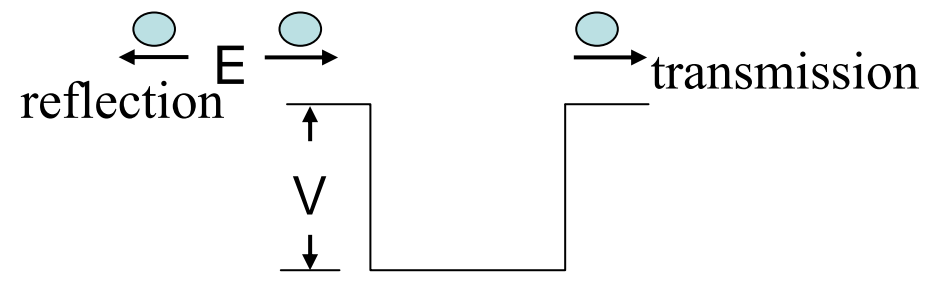
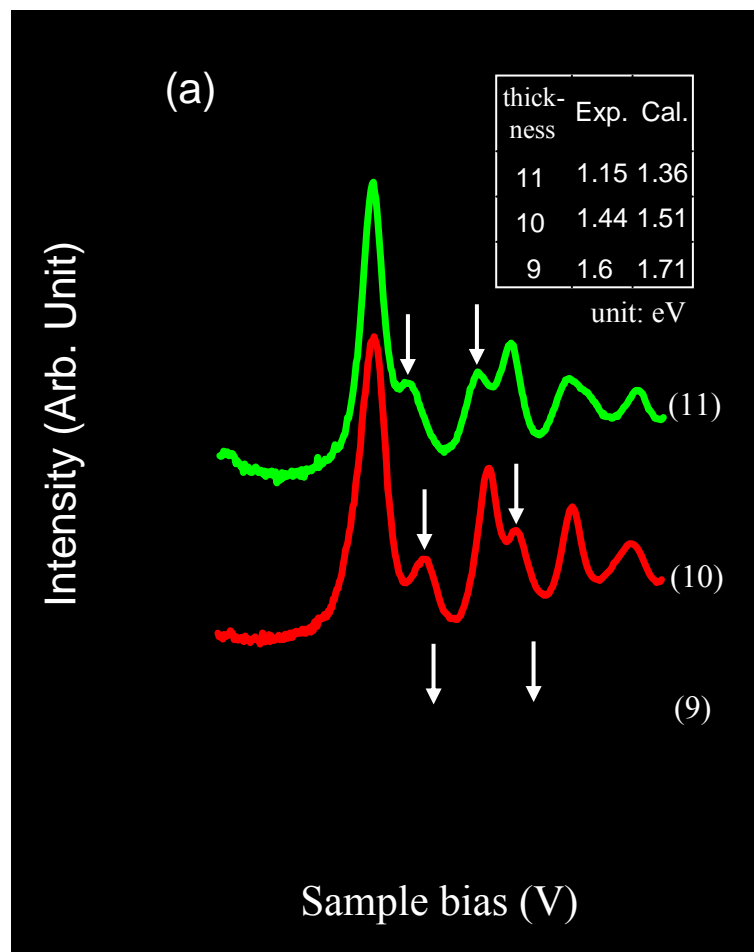
Transmission Resonance in Ag Films on Si(111)



Work function of Ag/Si(111) = 4.41 eV

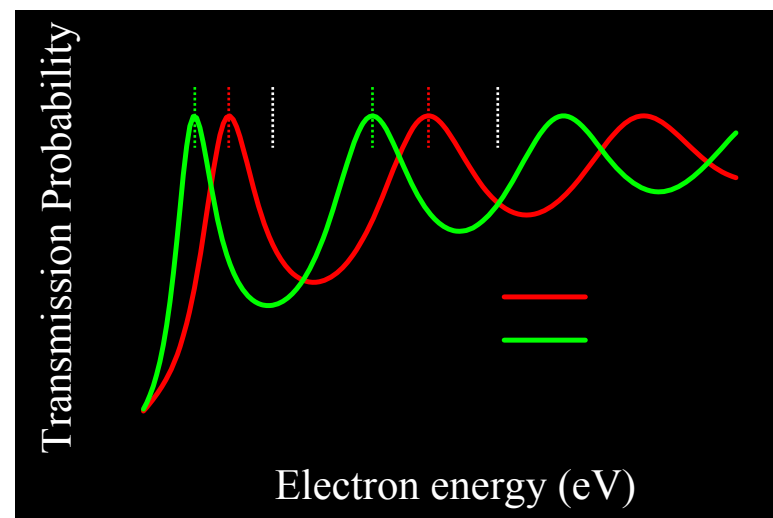


Quantum Size Effect above Vacuum Level



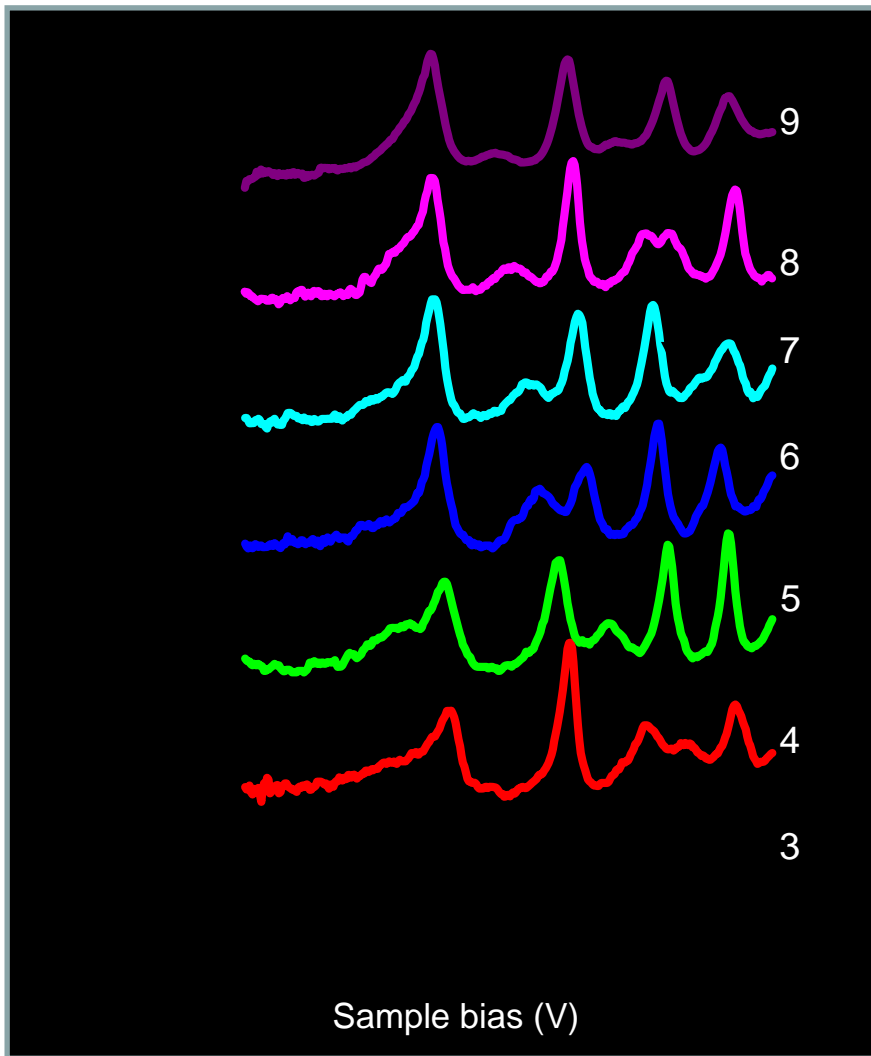
$$\frac{1}{T} = 1 + \frac{1}{4} \frac{V^2}{E(E+V)} \sin^2(kt); R = 1 - T; \frac{\hbar^2 k^2}{2m} = E + V$$

$kt = n\pi \rightarrow T = 1$ transmission resonance

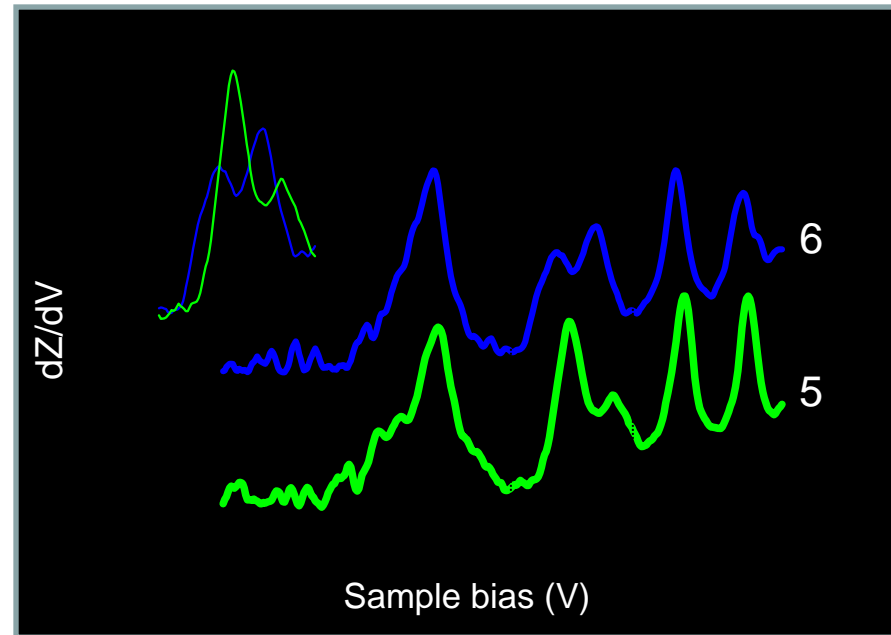
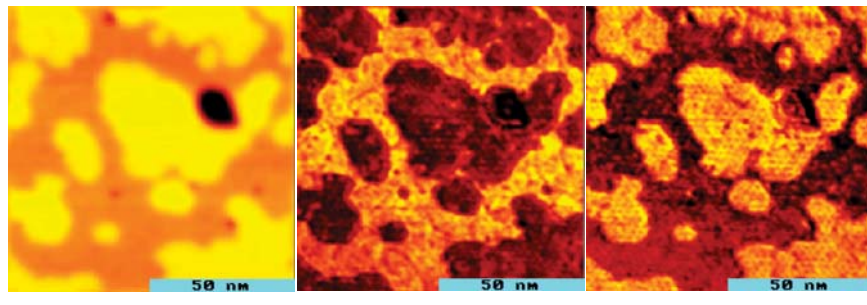




"Finger print" of film thickness



Low temperature deposition followed annealing to room temperature





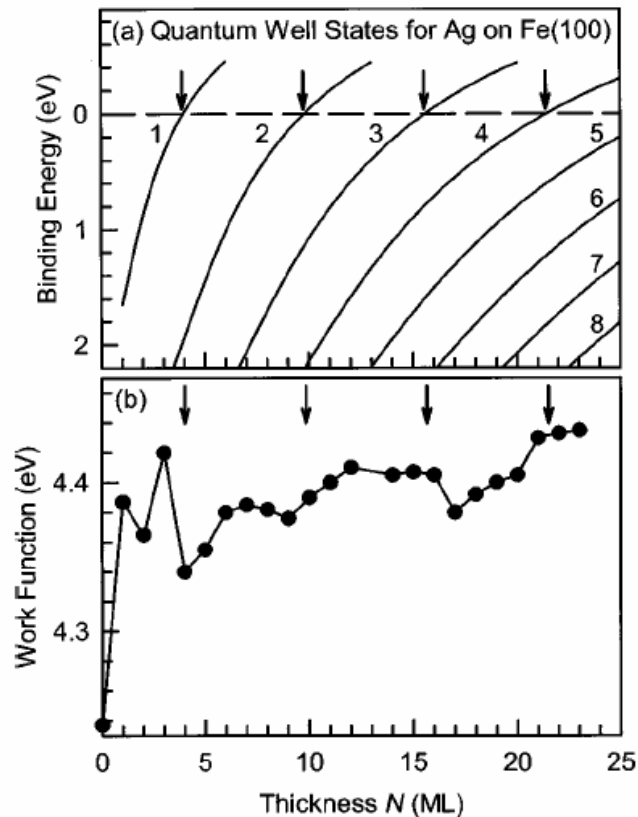
Summary

- *Quantum well states are measured with STS in the Pb films of varied thickness on the Si(111) surface.*
- *Quantum phenomenon of the transmission resonance can be observed with STS in Ag films on the Si(111) surface.*
- *Positions of the transmission resonance measured with STS can serve as finger prints for the Ag films of varied thickness.*



Work function measurements for thin films

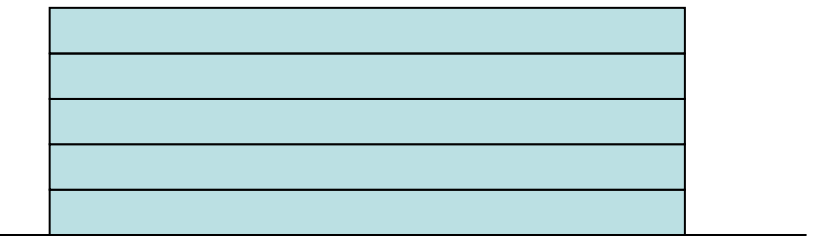
work function measurement for thin film using photo-emission spectroscopy



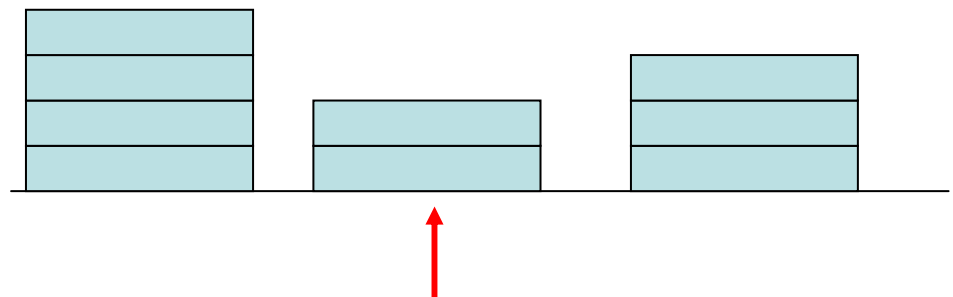
J. J. Paggel et al. 66, Phys. Rev. B (2002) 233403.

Broad beam technique

require layer by layer growth



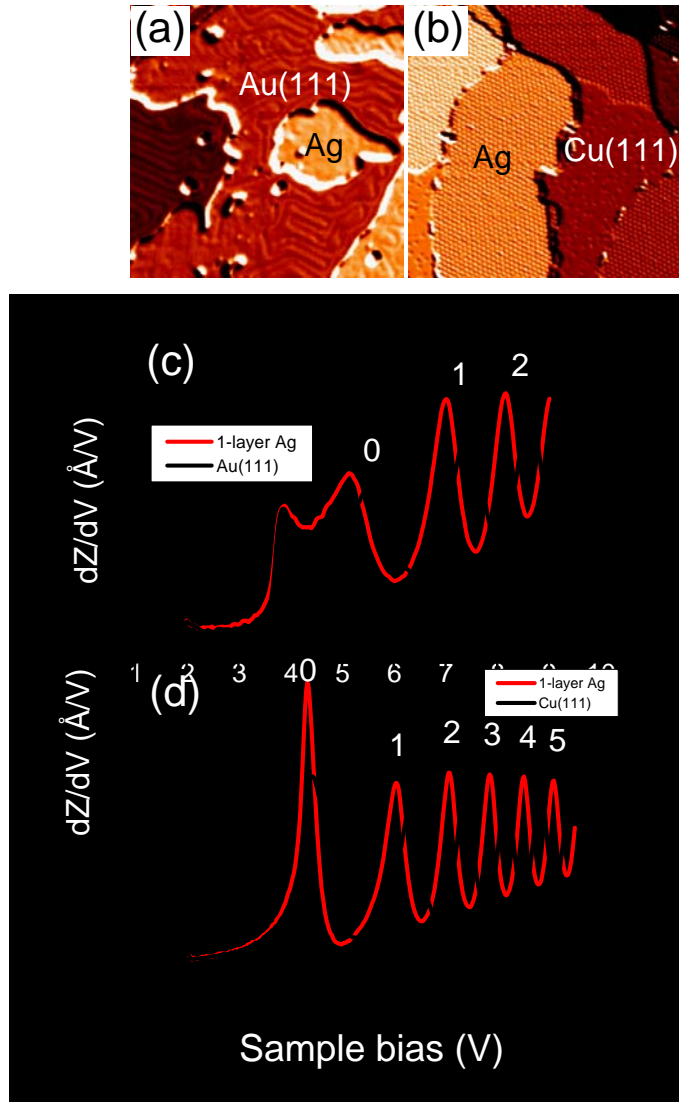
Average work function of various thickness



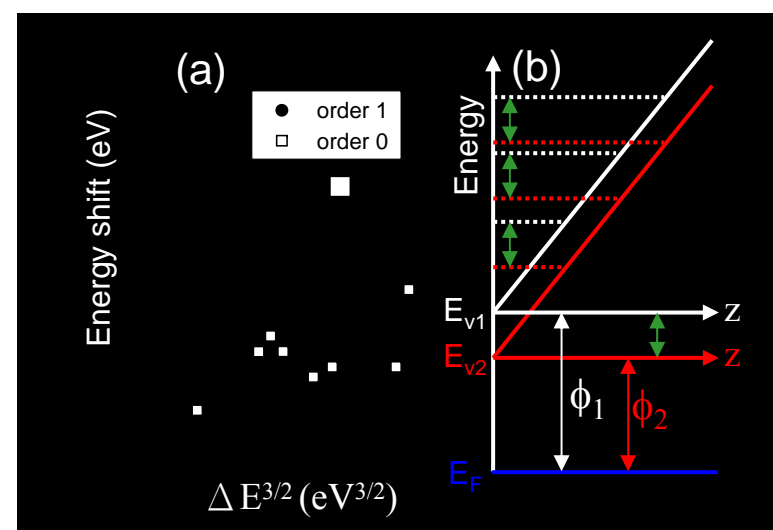
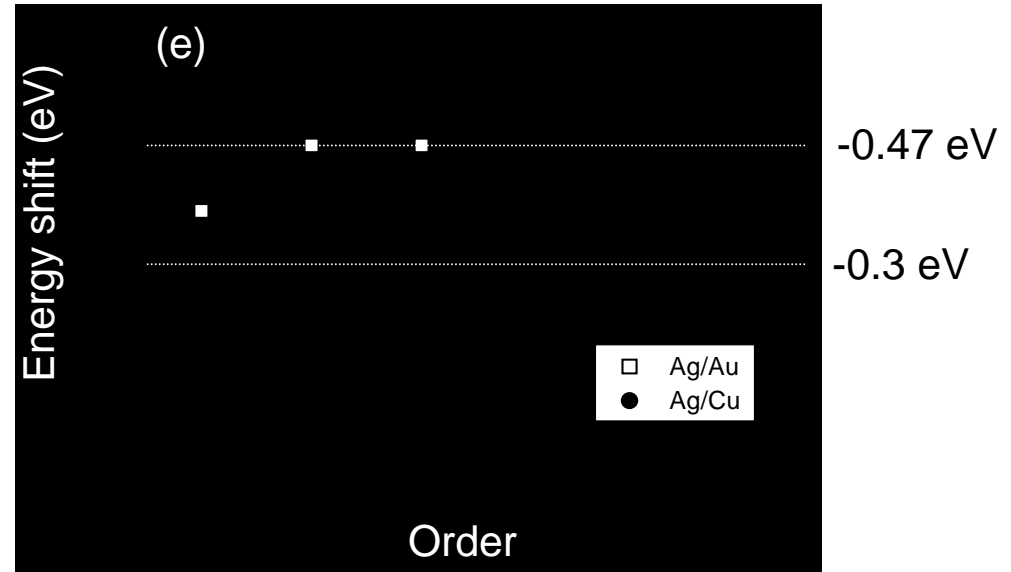
Local probe technique, e.g. STM

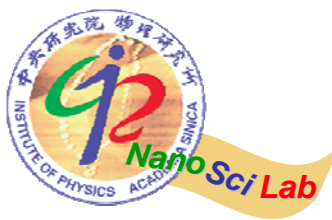


Constant Energy Shift



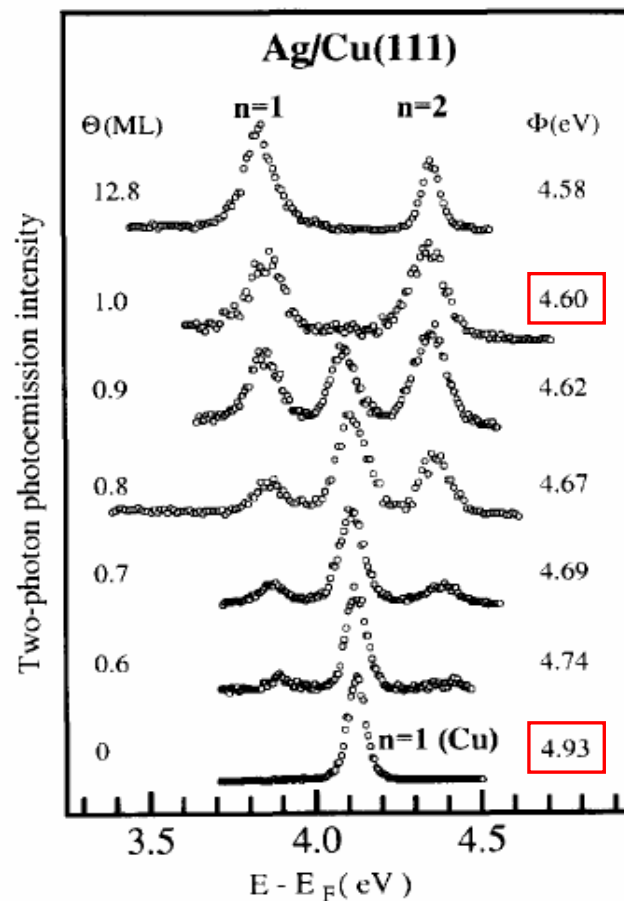
Lin et al., Phys. Rev. Lett. 99, 216103 (2007)





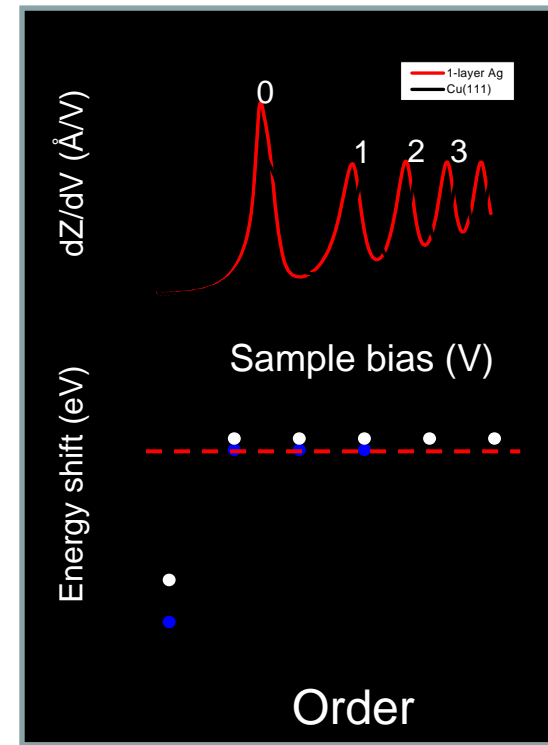
Comparison with PES measurement

Photoemission (-0.33 eV)



Wallauer et al., Surf. Sci 331, 731 (1995)

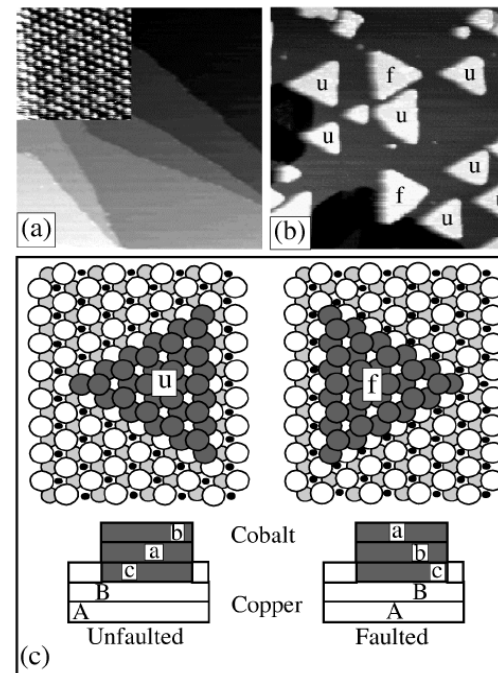
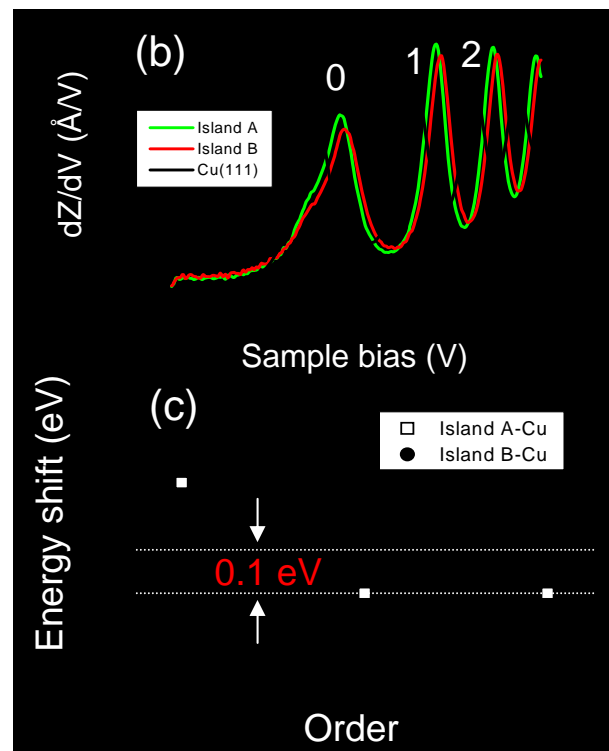
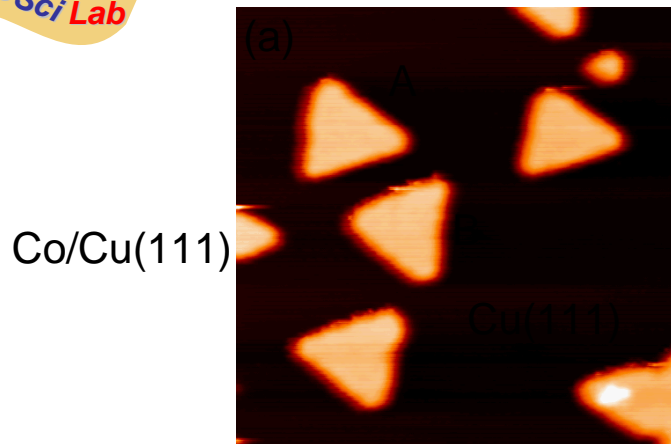
Gundlach oscillation (-0.3 eV)



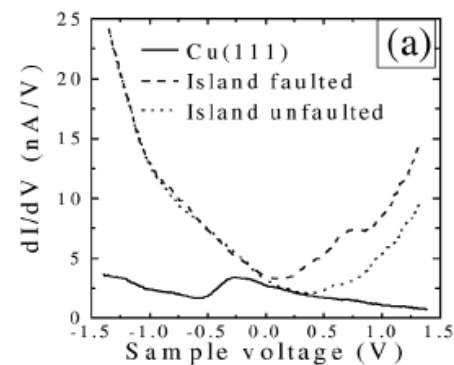
Bulk Materials	Φ (eV)
Au(111)	5.31
Ag(111)	4.74
Cu(111)	4.98



Detection of Subtle Variation of Work Function



Vázquez de Parga et al., Phys. Rev. Lett. **85**, 4365



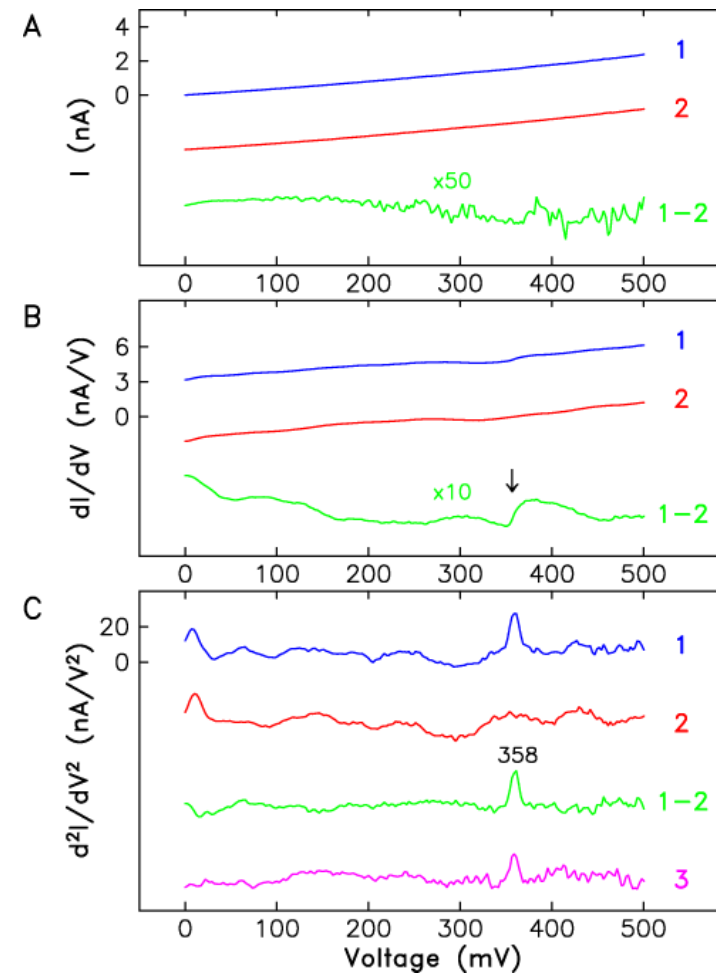
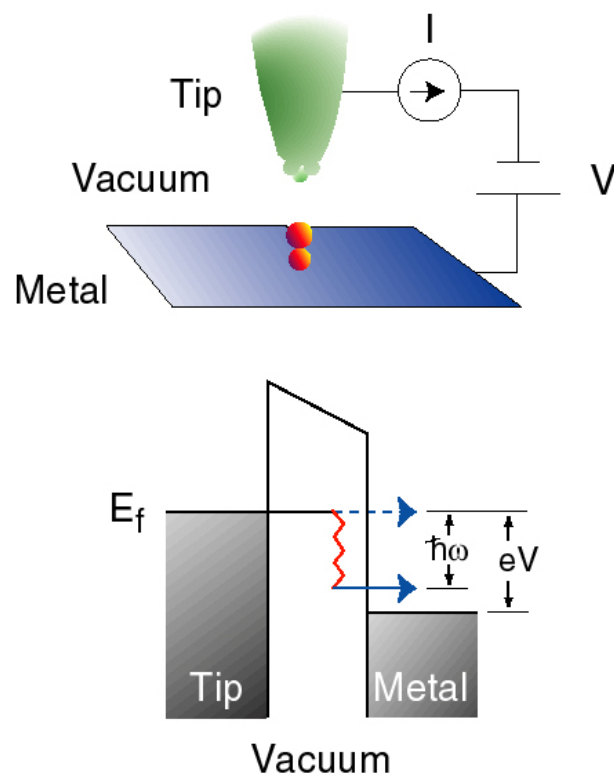


Summary

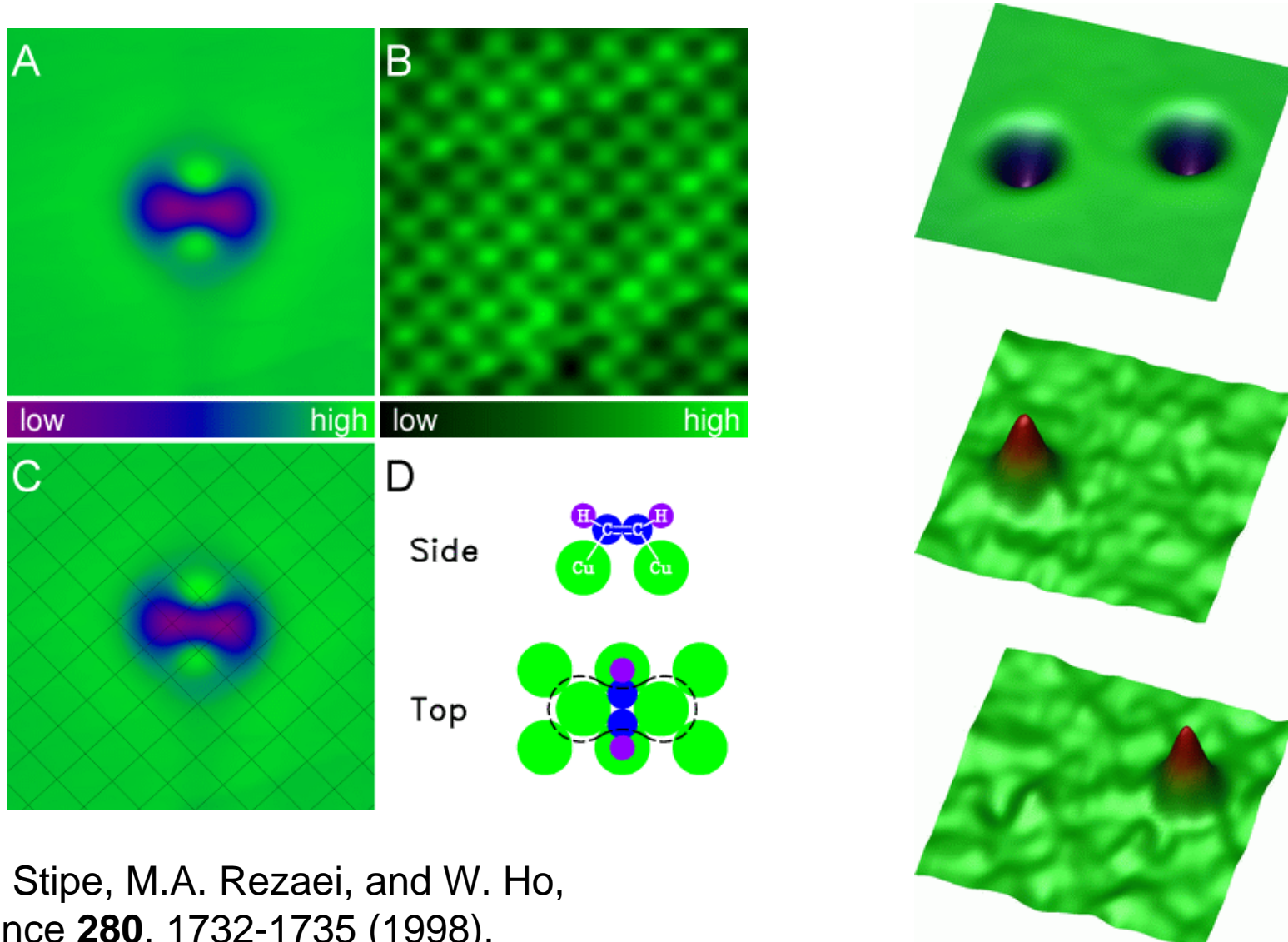
- *A general phenomenon of the constant energy shift is observed in high order Gundlach oscillation.*
- *The work function of a thin metal film can be measured with the constant energy shift.*
- *The precision of the measurement can be better than 0.02 eV, comparable to the photoemission results.*

Inelastic Tunneling

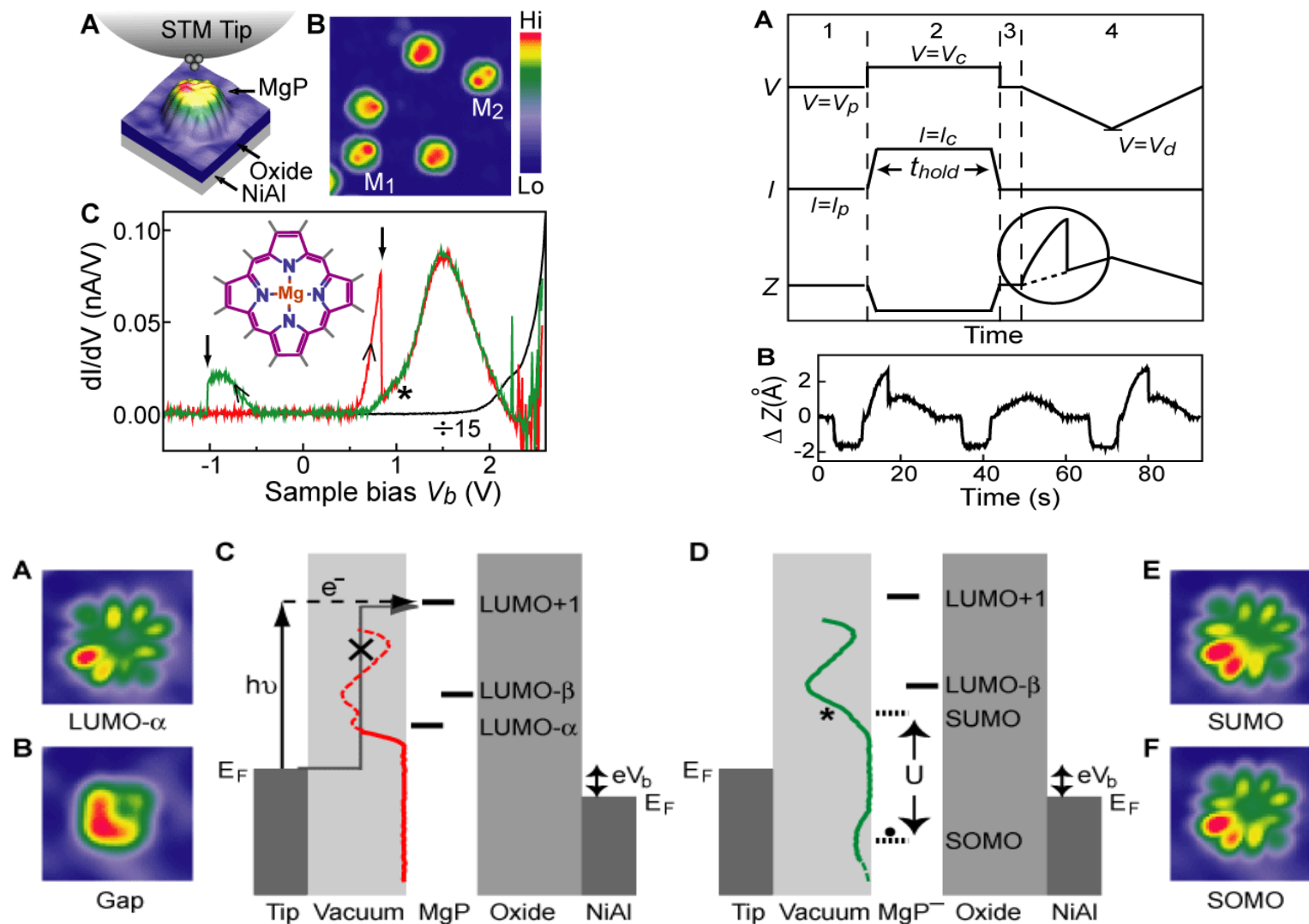
Elastic vs. Inelastic Tunneling



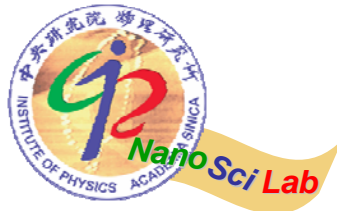
Single Molecule Vibrational Spectroscopy and Microscopy



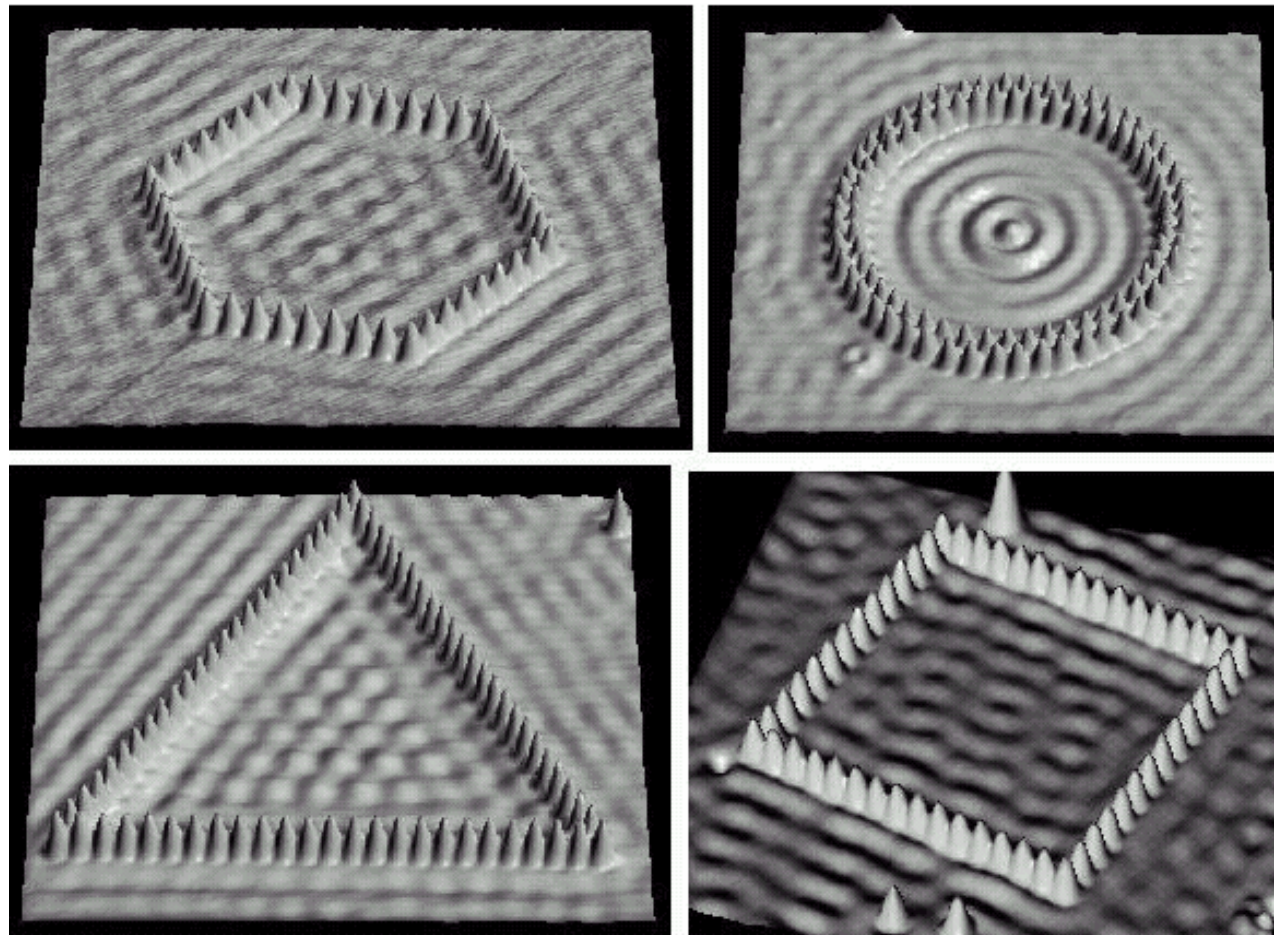
Atomic Scale Coupling of Photons to Single-Molecule Junctions



S.W. Wu and N. Ogawa and W. Ho, Science 312, 1362-1365 (2006)



Quantum corral



D.M. Eigler, IBM, Amaden

Artificial atom

